ATOMIC CLUSTERS AND NANOPARTICLES: COURSE 5

SEMICLASSICAL APPROACHES TO MESOSCOPIC SYSTEMS

MATTHIAS BRACK

Institute for Theoretical Physics,
University of Regensburg,
D-9304 Regensburg,
Germany

LES HOUCHES 2000, Session LXXIII

Contents

SEMICLASSICAL APPROACHES TO MESOSCOPIC SYSTEMS

Matthias Brack

Abstract

We review semiclassical methods of determining both average trends and quantum shell effects in the properties of finite fermion systems. *I. Extended Thomas-Fermi model (ETF):* The average, self-consistent mean field can be determined by density variational calculations using the semiclassical gradient-expanded ETF density functional for the kinetic energy. From this, average ground-state properties such as binding energies, densities, separation energies, etc. can be derived. *II. Periodic orbit theory (POT):* Quantum oscillations in a mean-field system can be obtained from the semiclassical trace formula that expresses the quantum-mechanical density of states in terms of the periodic orbits of the corresponding classical system. Only the shortest periodic orbits with highest degeneracy are important for the coarse-grained level density, i.e., for the gross shell effects. Particular uniform approximations are required to treat systems with mixed classical dynamics due to the effects of symmetry breaking and orbit bifurcations. *III. Local-current approximation (LCA):* The collective dynamics of the fermions can be described in linear-response theory, approximating the particle-hole excitation operators semiclassically by local current distributions. The method is suitable in combination with both the ETF density variational approach or with the Kohn-Sham density functional approach for the ground state, and allows one to describe optic response properties such as static polarizabilities and plasmon resonances. Applications of all methods to metal clusters and various mesoscopic nanostructures are given.

Published in:
NATO Advanced Study Institute, Les Houches, 2-28 July 2000
Session LXXIII: Atomic Clusters and Nanoparticles
Eds. C. Guet *et al.* (Springer-Verlag Berlin, 2001) pp. 161-219.

1 Introduction

We want to describe properties of finite fermion systems semiclassically. We start from a mean-field approach where the particles move independently in a selfconsistent potential. There are essentially two standard methods to derive such a selfconsistent potential (see, e.g., Ref. [1]): *i*) the Hartree-Fock (HF) theory in which the exchange is treated exactly, and *ii*) the Kohn-Sham (KS) density functional theory (DFT) in which the exchange often is treated only in the local density approximation (LDA), but other correlations can also be included. In the following, we write the mean-field Hamiltonian as the sum of the kinetic energy operator and the selfconsistent mean field V (that includes possible external fields)

$$\hat{H} = \hat{T} + V. \tag{1.1}$$

The single-particle energies ε_i and wavefunctions φ_i are given by the (HF or KS) Schrödinger equation

$$\hat{H}\varphi_i(\mathbf{r}) = \varepsilon_i\varphi_i(\mathbf{r})\,. \tag{1.2}$$

In HF theory, V contains also the non-local Fock exchange term, whereas in KS-DFT theory, $V = V(\mathbf{r})$ is a *local* potential (the total KS potential, which includes also an exchange-correlation part). For simplicity we assume that the spectrum ε_i is discrete.

The fundamental quantity that contains all the quantum information of the energy spectrum is the single-particle *level density*

$$g(E) = \mathrm{tr}\,\delta(E-\hat{H}) = \sum_i \langle i|\delta(E-\hat{H})|i\rangle = \sum_i \delta(E-\varepsilon_i)\,, \tag{1.3}$$

where $\delta(x)$ is the Dirac delta function. The summation over i here goes over the complete spectrum including all degeneracies.

Following very general arguments of Strutinsky [2], the level density may be split into an average part $\widetilde{g}(E)$ and an oscillating part $\delta g(E)$:

$$g(E) = \widetilde{g}(E) + \delta g(E)\,. \tag{1.4}$$

Although the two parts arise naturally within the periodic orbit theory (POT), as will be discussed in Section 3, it is customary to consider them separately. The average part $\widetilde{g}$ may be calculated numerically from the ε_i by the Strutinsky averaging method [2]. It is equivalent [3,4] to its semiclassical approximation obtained in the extended Thomas-Fermi (ETF) model which will be discussed in Section 2. The oscillating part δg, which contains all the quantum shell effects coming from the non-uniform distribution of the single-particle levels ε_i (including their degeneracies), is obtained semiclassically in the POT discussed explicitly and illustrated in Section 3. A semiclassical approach to the *collective* excitation spectrum, using a local-current approximation (LCA), is finally presented in Sect. 4.

2 Extended Thomas-Fermi model for average properties

The ETF model allows one to obtain average properties such as binding and deformation energies, separation energies, etc., that do not include quantum oscillations. The main idea of the TF model is to take an average over the classical phase space with a unit occupation probability per unit cell h^3, where h is Planck's constant (we assume in the following a 3-dimensional system), multiplied by a factor 2 to take the spin degeneracy into account. Including finite $\hbar$-correction terms yields the extended TF model that contains average quantum corrections without, however, generally allowing for quantum shell effects.

2.1 Thomas-Fermi approximation

The TF approximation for the level density is obtained by taking the trace in (1.3) in the phase space:

$$g_{TF}(E) = \frac{2}{h^3}\int \delta[E - H_{cl}(\mathbf{r},\mathbf{p})]\, d^3r\, d^3p\,, \tag{2.1}$$

where we have replaced $\hat{H}$ by the classical Hamiltonian H_{cl}

$$H_{cl}(\mathbf{r},\mathbf{p}) = \frac{1}{2m}\mathbf{p}^2 + V(\mathbf{r})\,. \tag{2.2}$$

If the mean field in (1.1) contains non-local terms (e.g., the Fock term in the case of HF theory), then the potential will also be momentum dependent, $V = V(\mathbf{r},\mathbf{p})$, and can be obtained from (1.1) by a Wigner transform [1]. In the following we assume $V(\mathbf{r})$ to be local and analytical. In the ground state of a mean-field system, all levels up to the Fermi energy E_F are occupied. The total number of particles N is then given by the integral

$$N = \int_0^{E_F} g(E)\, dE = \frac{2}{h^3}\int \Theta[E_F - H_{cl}(\mathbf{r},\mathbf{p})]\, d^3r\, d^3p\,, \tag{2.3}$$

where $\Theta(x)$ is the Heavyside step function. The momentum integration can be done immediately with (2.2), using its spherical symmetry in momentum space, and yields

$$N = \frac{1}{3\pi^2}\left(\frac{2m}{\hbar^2}\right)^{3/2}\int [E_F - V(\mathbf{r})]^{\,3/2}\, d^3r\,. \tag{2.4}$$

Omitting the spatial part of the integral in (2.4) yields the TF approximation of the spatial density:

$$\rho_{TF}(\mathbf{r}) = \frac{1}{3\pi^2}\left(\frac{2m}{\hbar^2}\right)^{3/2}[E_F - V(\mathbf{r})]^{\,3/2}\,\Theta[E_F - V(\mathbf{r})]\,. \tag{2.5}$$

Note the step function which implies that the TF density is zero outside the classical turning points $\mathbf{r}_i$ defined by $E_F = V(\mathbf{r}_i)$. In the same way we can also obtain the total kinetic energy E_{kin} of the system by the integral

$$E_{kin} = \frac{2}{h^3} \int \frac{p^2}{2m}\, \Theta[E_F - H_{cl}(\mathbf{r},\mathbf{p})]\, d^3r\, d^3p \tag{2.6}$$

which after momentum integration yields

$$E_{kin} = \frac{1}{5\pi^2} \left(\frac{2m}{\hbar^2}\right)^{3/2} \int [E_F - V(\mathbf{r})]^{\,5/2}\, d^3r\,, \tag{2.7}$$

so that the kinetic energy density becomes

$$\tau_{TF}(\mathbf{r}) = \frac{1}{5\pi^2} \left(\frac{2m}{\hbar^2}\right)^{3/2} [E_F - V(\mathbf{r})]^{\,5/2}\, \Theta[E_F - V(\mathbf{r})]\,. \tag{2.8}$$

From Eqs. (2.5,2.8) we can eliminate the Fermi energy and the potential to obtain the TF functional for the kinetic energy density

$$\tau_{TF}[\rho] = \frac{\hbar^2}{2m}\, \kappa\, \rho^{\,5/3}\,, \qquad \text{with} \quad \kappa = \frac{3}{5}\,(3\pi^2)^{\,2/3}. \tag{2.9}$$

Eqs. (2.5) and (2.8,2.9) are the expressions which were used by Thomas and Fermi [5] to describe the electronic density and energy of the atom semiclassically in a selfconsistent way (see, e.g., the book by N. March [6] for a very nice presentation). Although the TF model gives a nice qualitative description of the average properties of an atom, it is not very good. (It has been shown, though, that the total TF energy for the neutral atom becomes *exact* in the mathematical limit of infinite nuclear charge $Z \to \infty$; see Ref. [7] for a review.) It is possible, however, to improve the TF model by taking into account a series of quantum corrections, leading to the so-called "extended Thomas-Fermi" (ETF) model which we will summarize in the following subsections.

2.2 Wigner-Kirkwood expansion

There are various ways to derive the quantum corrections to the TF model; we use the method developed by Wigner and Kirkwood [8] which starts from expansion in powers of $\hbar$ of the single-particle Bloch density matrix around its classical TF value. We refer to a recent monograph [4] for a detailed presentation of this method and summarize just the general idea and results. The basic idea is to relate the quantities of interest to the Bloch density matrix which is defined as the statistical operator $e^{-\beta\hat{H}}$ in coordinate-space representation:

$$C(\mathbf{r},\mathbf{r}';\beta) = \sum_i \varphi_i^*(\mathbf{r}')\, \varphi_i(\mathbf{r})\, e^{-\beta\varepsilon_i} = \langle \mathbf{r}|e^{-\beta\hat{H}}|\mathbf{r}'\rangle\,, \tag{2.10}$$

where the sum goes again over the complete spectrum. Here β is a complex mathematical variable. The inverse Laplace transform (see, e.g, Refs. [9,10]) of $C(\mathbf{r},\mathbf{r}';\beta)$ yields the single-particle density matrix

$$\begin{aligned}\rho(\mathbf{r},\mathbf{r}') &= \sum_{\varepsilon_i\le E_F} \varphi_i^*(\mathbf{r}')\,\varphi_i(\mathbf{r}) \;=\; \mathcal{L}^{-1}_{E_F}\left[\frac{1}{\beta}C(\mathbf{r},\mathbf{r}';\beta)\right] \\ &= \frac{1}{2\pi i}\int_{c-i\infty}^{c+i\infty}\frac{1}{\beta}\,C(\mathbf{r},\mathbf{r}';\beta)\,e^{\beta E_F}\,d\beta\,. \qquad (c>0) \end{aligned} \tag{2.11}$$

From this one obtains easily the local density

$$\rho(\mathbf{r}) = \sum_{\varepsilon_i\le E_F}|\varphi_i(\mathbf{r})|^2 = \rho(\mathbf{r},\mathbf{r}) \tag{2.12}$$

and the kinetic energy density

$$\tau(\mathbf{r}) = -\frac{\hbar^2}{2m}\sum_{\varepsilon_i\le E_F}\varphi_i^*(\mathbf{r})\,\Delta\varphi_i(\mathbf{r}) = -\frac{\hbar^2}{2m}\,\Delta_{\mathbf{r}}\rho(\mathbf{r},\mathbf{r}')|_{\mathbf{r}'=\mathbf{r}}, \tag{2.13}$$

where the subscript $\mathbf{r}$ here and in the following indicates that an operator acts only on the variable $\mathbf{r}$ on its right. Note that these are so far the exact quantum-mechanical expressions. The TF approximation and its extensions may now be obtained in the following way. Take the matrix element in (2.10) in a plane-wave representation (including the spin factor 2):

$$C(\mathbf{r},\mathbf{r}';\beta) = \frac{2}{h^3}\int d^3p\; e^{-i\mathbf{p}\cdot\mathbf{r}'/\hbar}\,e^{-\beta\hat{H}_{\mathbf{r}}}\,e^{i\mathbf{p}\cdot\mathbf{r}/\hbar}\,. \tag{2.14}$$

Due to the potential $V(\mathbf{r})$ in (1.1), the plane waves are no eigenfunctions of $\hat{H}$. If we replace $\hat{H}_{\mathbf{r}}$ in the exponent above by the classical Hamilton function $H_{cl}(\mathbf{r},\mathbf{p})$ and perform the $\mathbf{p}$ integration, we obtain the classical Bloch density matrix

$$C_{cl}(\mathbf{r},\mathbf{r}';\beta) = 2\left(\frac{m}{2\pi\hbar^2\beta}\right)^{3/2}\exp\left[-\beta V(\mathbf{r}) - \frac{m}{2\hbar^2\beta}(\mathbf{r}-\mathbf{r}')^2\right]. \tag{2.15}$$

Inserting this into Eq. (2.11) yields the TF densities. To obtain quantum corrections to the TF results, one starts from the ansatz

$$e^{-\beta\hat{H}}\,e^{i\mathbf{p}\cdot\mathbf{r}/\hbar} = e^{-\beta H_{cl}(\mathbf{r},\mathbf{p})}\,e^{i\mathbf{p}\cdot\mathbf{r}/\hbar}\,w(\mathbf{r},\mathbf{p};\beta)\,, \tag{2.16}$$

and expands $w(\mathbf{r},\mathbf{p};\beta)$ into a series in powers of $\hbar$:

$$w = 1 + \hbar w_1 + \hbar^2 w_2 + \ldots \tag{2.17}$$

Hereby the w_n are functions of $\mathbf{r}$, $\mathbf{p}$, and β, containing up to n gradients acting on the potential $V(\mathbf{r})$. The series (2.17) may, e.g., be obtained by expanding the left side of Eq. (2.16) in terms of repeated commutators of the kinetic energy operator with $V(\mathbf{r})$ (see Ref. [1]). Another way, solving iteratively a differential equation for $w(\mathbf{r},\mathbf{p};\beta)$ (the so-called Bloch equation), is described in Ref. [4]. Only the even terms of the series (2.17) with $n = 2m$, $m = 1, 2, 3, \ldots$ survive the $\mathbf{p}$ integration for the local density and kinetic energy density, and give the ETF corrections to (2.5) and (2.8). These correction terms diverge at the classical turning points, but they can be integrated to yield finite corrections to the particle number, the total energies and other integrated quantities. The densities obtained in this way by truncation of the series (2.17) at some order are usually called the ETF densities $\rho_{ETF}(\mathbf{r})$ and $\tau_{ETF}(\mathbf{r})$ (see, e.g., Ref. [4] for their explicit forms).

2.3 Gradient expansion of density functionals

Eliminating the potential and its gradients from the ETF densities, which takes some algebra (cf. Ref. [11] where this has been done systematically also for momentum and spin dependent potentials), one arrives at the kinetic energy-density functional $\tau_{ETF}[\rho]$ including gradient correction terms. We quote here only its integrated form as it contributes to the total kinetic energy functional $T_{ETF}[\rho]$. Keeping terms up to fourth order in $\hbar$ one obtains after some partial integrations [12, 13]

$$E_{kin} \;=\; T_{ETF}[\rho] \;=\; \frac{\hbar^2}{2m}\int d^3r\,\left\{\kappa\rho^{\,5/3} + \frac{1}{36}\frac{(\nabla\rho)^2}{\rho}\right. \tag{2.18}$$
$$\left. + \frac{1}{6480}(3\pi^2)^{-2/3}\rho^{\,1/3}\left[8\left(\frac{\nabla\rho}{\rho}\right)^4 - 27\left(\frac{\nabla\rho}{\rho}\right)^2\frac{\Delta\rho}{\rho} + 24\left(\frac{\Delta\rho}{\rho}\right)^2\right]\right\}.$$

In the first term of (2.18) we recognize the TF functional (2.9). The second term, coming from the $\hbar^2$ corrections, has been derived for the first time by von Weizsäcker [14], albeit with a different coefficient. Eq. (2.18) has the correct coefficient in the limit of slowly varying densities, whereas the original Weizsäcker coefficient (1/4 instead of 1/36) is correct in the limit of rapid density oscillations with small amplitude (see Ref. [15] for a detailed discussion). The terms shown on the second line in (2.18) come from the $\hbar^4$ terms of the semiclassical expansion (2.17). Although the derivation of the functional (2.18) sketched above is valid only within the classically allowed region, it can be shown from its extension to finite temperature [16, 17], where the ETF densities stay finite and are defined in the whole space, that the zero-temperature limit leads to Eq. (2.18) also in the classically forbidden region (see also Refs. [18, 19]).

The functional (2.18) is only expected to be correct for average densities without quantum shell oscillations, since it has been derived in a semiclas-

sical framework that has no room for shell effects. Nevertheless, it has been used in connection with atomic HF densities [20] and found to reproduce the total kinetic energies quite well. A careful study of (2.18) using numerically Strutinsky-averaged quantum-mechanical densities $\widetilde{\rho}(\mathbf{r})$ for various forms of the potential $V(\mathbf{r})$ was done in Ref. [21]. The Strutinsky-averaged kinetic energies $\widetilde{T}$ were found to be well reproduced when all terms up to fourth order in (2.18) were taken into account, as is demonstrated in Fig. 1. The dashed curve in the right panel of the figure shows the exact quantum-mechanical kinetic energy which exhibits pronounced shell effects; the ETF functional (2.18) clearly serves to reproduce only the *average* part of the kinetic energy.

Similarly, one obtains also gradient corrections to the exchange-correlation energy functional occurring in DFT [1], or corrections arising in connec-

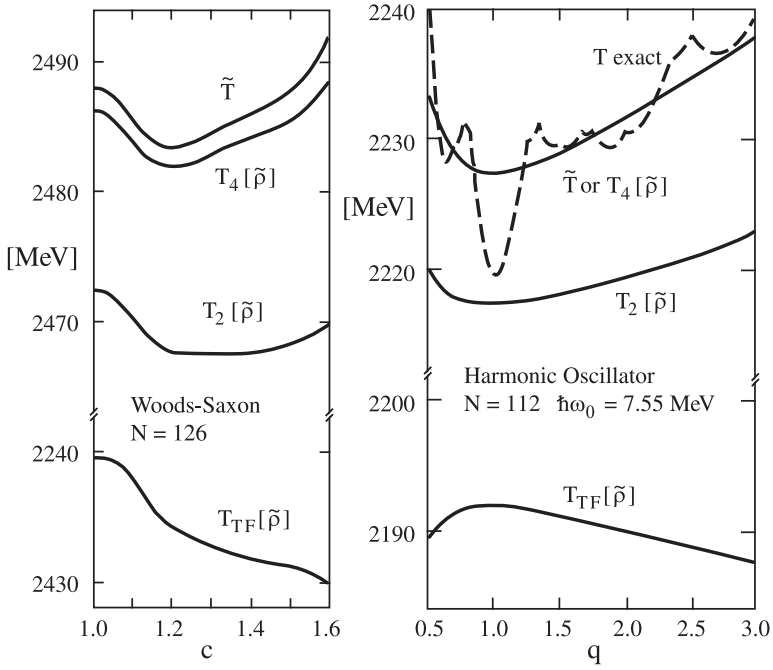

Fig. 1. Tests of the kinetic energy functional $\tau_{ETF}[\rho]$ (2.18). *Left:* Deformed Woods-Saxon potential with $N = 126$ nucleons (after [13]; see the definition there of the deformation parameter c). *Right:* Axially symmetric harmonic-oscillator potential with frequency ratio q with $N = 112$ particles (after [21]). The index in $T_{2m}[\widetilde{\rho}]$ gives the maximum order of $\hbar$ corrections included ($m = 0$ is TF). $\widetilde{T}$ is the Strutinsky-averaged kinetic energy (not distinguishable from $T_4[\widetilde{\rho}]$ on the r.h. side). Note the shell effects in the exact kinetic energy T shown by a dashed line.

tion with nonlocal potentials (e.g., spin-orbit and effective mass terms; see Ref. [19] for the case of effective Skyrme interactions in nuclear physics). Note that nonlocal potentials give also corrections to the kinetic energy functional (2.18) [11, 19]. Relativistic functionals $T_{ETF}[\rho]$ have also been derived [1, 22, 23].

2.4 Density variational method

Within the framework of the density functional theory (DFT), the Hohenberg-Kohn theorem [24] tells us that the total energy of a fermion system is uniquely given as a functional of the local density $\rho(\mathbf{r})$. We write it here as the sum of kinetic and potential parts:

$$E_{tot} = T_s[\rho] + E_{pot}[\rho] = \int \{\tau(\mathbf{r}) + \mathcal{E}_{pot}[\rho]\}\; d^3r\,, \tag{2.19}$$

where $T_s[\rho]$ is the kinetic energy of a non-interacting system with density $\rho(\mathbf{r})$ and $E_{pot}[\rho]$ the sum of all potential energy terms including the contribution from any external one-body potential $V_{ext}(\mathbf{r})$, which just gives a term $V_{ext}(\mathbf{r})\rho(\mathbf{r})$ under the integral above, and the exchange-correlation energy (that also takes into account the interacting part of the kinetic energy, see Ref. [1]). The exact functional $T_s[\rho]$ is not explicitly known; therefore one has to express it via $\tau(\mathbf{r})$ in Eq. (2.13) in terms of single-particle wavefunctions $\varphi_i(\mathbf{r})$ and vary the total energy with respect to these, which leads to the Kohn-Sham (KS) equations.

If we are not interested in the quantum shell effects, we can replace $T_s[\rho]$ by the semiclassical ETF functional (2.18), so that the energy (2.19) becomes an explicit functional of $\rho(\mathbf{r})$. We can then directly apply the variational principle by making $E[\rho]$ stationary with respect to an arbitrary local variation $\delta\rho(\mathbf{r})$ of the (average) density. To keep the number of particles N constant we include a Lagrange multiplier μ which is just the Fermi energy of the average system. This yields the Euler-Lagrange variational equation

$$\frac{\delta}{\delta\rho(\mathbf{r})}\left[E[\rho(\mathbf{r})] - \mu\int \rho(\mathbf{r})\, d^3r\right] = 0\,. \tag{2.20}$$

Its solution gives the *average* ground-state energy and density of the system within the ETF approximation. To keep the notation simple, we still write $\rho(\mathbf{r})$ but keep in mind that $\rho(\mathbf{r})$ and $E[\rho]$ only represent the average quantities. The variation of the potential energy gives, quite generally, the local mean-field potential $V(\mathbf{r})$ which depends in a selfconsistent way on the density itself

$$\frac{\delta}{\delta\rho(\mathbf{r})}E_{pot}[\rho(\mathbf{r})] = V[\rho(\mathbf{r})]\,. \tag{2.21}$$

$V[\rho]$ is formally identical to the total KS potential (except that it is evaluated here for the average density); it depends, of course, on the particular

system under consideration and on the two-body interaction. The variation of the kinetic energy part, however, is universal and can be calculated directly from the explicit form of the ETF functional given above. To avoid lengthy formulae, we give here explicitly only the result obtained up to the Weizsäcker term. Assuming the density variation $\delta\rho(\mathbf{r})$ to vanish on the boundary (which usually is at infinity) and using the standard techniques of variational calculus, one gets the following differential equation

$$\frac{\hbar^2}{2m}\left\{\frac{5}{3}\kappa\rho^{2/3}+\frac{1}{36}\left[\frac{(\nabla\rho)^2}{\rho^2}-2\frac{\nabla^2\rho}{\rho}\right]\right\}+D_4[\rho]+V[\rho]=\mu\,, \qquad (2.22)$$

where D_4 is the contribution from the fourth-order gradient term, $D_4[\rho] = \delta T_4[\rho]/\delta\rho$, whose explicit form (containing seven terms with up to fourth-order gradients of ρ) may be found in Ref. [19]. Equation (2.22) is a partial differential equation which in general can only be solved numerically. To lowest TF order, neglecting all gradient terms, the solution of (2.22) for the density $\rho(\mathbf{r})$ is algebraic and gives, as it should, exactly the TF density $\rho_{TF}(\mathbf{r})$ given in (2.5).

If the gradient terms are kept in Eq. (2.22), the nature of the solutions depends on the behaviour of the potential $V(\mathbf{r})$. For the following discussions and applications, we shall assume that $V(\mathbf{r})$ is finite in the interior of the system and goes to zero at large distances. Then the asymptotic fall-off of the density is always governed by the highest gradient term included in the variational equation (2.22). (See Ref. [1] for the problems that arise in atomic systems from the $1/r$ divergence at the center due to the external nuclear potential.) Keeping just the Weizsäcker term, the solutions for the density are found to decay exponentially. This is because the constant Fermi energy μ can only be cancelled by the highest gradient term in Eq. (2.22). The rate of the exponential fall-off turns, however, out to be too fast in comparison to that of exact quantum-mechanical densities. One pragmatic way out of this problem is to artificially increase the coefficient of the Weizsäcker term, adjusting it by optimizing the results. The dilemma hereby is that the same constant cannot be used for densities and for integrated energies. Nevertheless, this procedure has been widely used in physics and physical chemistry (see Ref. [1] for details and applications). It violates, however, the aspect of universality which is one of the nice features of the ETF model, and can easily be avoided by including the higher-order gradient terms in Eq. (2.22).

Including the fourth-order contribution $D_4[\rho]$, the density of a spherical system falls off only with the sixth inverse power of r, i.e., $\rho(r) \sim r^{-6}$. More generally, the highest derivative term in $\tau_{2m}[\rho]$ goes radially like [21]

$$\tau_{2m}[\rho(r)] \sim [\rho(r)]^{(5-2m)/3}\,\frac{1}{\rho(r)}\frac{d^{2m}\rho(r)}{dr^{2m}}\,, \qquad (2.23)$$

and the solution of Eq. (2.20) is found to fall off like

$$\rho(r) \sim r^{-3m/(m-1)} \quad \text{for} \quad r \to \infty\,. \qquad (m \geq 2) \qquad (2.24)$$

Inserting this into (2.23), one finds that the selfconsistent kinetic energy density $\tau(r)$ goes to zero with the same power law as $\rho(r)$ in (2.24). It can therefore always be integrated to give a finite kinetic energy. [The fact that the sixth- and higher-order gradient corrections to $\tau_{ETF}[\rho]$ yield diverging integrals for densities that decay exponentially like $\rho(r) \sim e^{-ar}$ has repeatedly been noted in the literature and interpreted as a break down of the ETF gradient expansion. This is an erroneous conclusion, since the selfconsistent solutions of (2.22) for $m > 2$ do *not* fall off exponentially.]

The inverse power law (2.24) found for $m \geq 2$ is, of course, not realistic for most systems, as the quantum-mechanical density usually falls of exponentially. It has turned out, however, that the asymptotic solution (2.24) is reached only mathematically very far away from the actual surface of a realistic system, and that the inclusion of the fourth-order term definitely improves the variational results. This has been shown in numerical solutions of the ETF variational equation (2.22) up to fourth order, both for atomic nuclei [18,25] and for metallic clusters within the jellium model [26]. Spherical symmetry was assumed in both cases so that the differential equation was only one-dimensional. The applications to metal clusters will be discussed explicitly in the remainder of this section.

One basic problem of the ETF variational method is that there is effectively no lower bound to the total energy, different from the Hartree-Fock method where this is granted by the Ritz principle. *A priori*, the Hohenberg-Kohn theorem [24] tells us that the total energy (2.19) has its variational minimum at the value of the exact energy of the system. But this holds only true if the *exact* density functional $E[\rho]$ is used which, however, is unknown. Due to the approximations necessary to put the density functional method into use – and here in particular due to the ETF approximation – this lower bound is no longer given. As a consequence, the variational ETF results are typically overbound, i.e., the (absolute) binding energies are too large [19,25]. The amount of overbinding in nuclei is, however, much smaller than one percent of the total energy.

We should like to emphasize again that due to the very nature of the ETF model, the Euler equation (2.22) cannot reproduce any of the quantum shell oscillations typical of finite fermion systems. The ETF variational method is thus limited to yield average properties of finite fermion systems. A perturbative way to include the shell effects, without going through the fully self-consistent microscopic HF or KS scheme, makes use of Strutinsky's shell-correction method (see Ref. [4]).

The extension of the ETF model to systems at finite temperature that can be described by a grand-canonical ensemble is straightforward, though

algebraically quite tedious. We refer to the literature [4, 17, 18] for its presentation and, in particular, to Ref. [18] where the functional $T_{ETF}[\rho]$ with its explicitly temperature-dependent coefficients can be found, as well as applications to nuclear physics. An example of the results obtained there is given in Fig. 5 below.

2.5 Applications to metal clusters

2.5.1 Restricted spherical density variation

The numerical solution of the nonlinear fourth-order differential equation (2.22) becomes very difficult, if not practically impossible, for deformed systems without symmetry. For that case one may perform the variation in (2.20) not exactly in $\mathbf{r}$ space, but in a restricted space of parameterized variational densities. The choice of the variational density is then a matter of physical intuition and, of course, not free of a certain bias. A spherical density profile that has proved useful for both nuclei [19] and metal clusters [27, 28] is a generalized Fermi function:

$$\rho(r) = \frac{\rho_0}{\left[1 + \exp\left(\frac{r-R}{a}\right)\right]^\gamma} \,. \tag{2.25}$$

Of the four parameters above, only three are independent due to the constraint of the particle number conservation. The independent parameters are then determined variationally by minimizing the total energy of the system under consideration, and no adjustable parameter is used anywhere. With this restricted variational procedure up to fourth order in the ETF functionals, density profiles and energies were obtained that agree very closely with the fully variational ETF results [25, 26] on one hand (see the following subsection), and with the averaged results of fully microscopic KS calculations for metal clusters [29, 30] and HF calculations for nuclei [19, 25] on the other hand. In particular, the profiles of the variationally optimized densities (2.25) match the selfconsistent quantum-mechanical ones over the entire region of the surface, demonstrating that the mathematically inadequate asymptotic inverse-power decays (2.24) of the exact solutions of (2.22) have no practical significance.

As an example we show in Fig. 2 the densities and potentials obtained in a large sodium cluster within the spherical jellium model (see, e.g., Ref. [31] for a detailed discussion of this model), both by solving the fully quantum-mechanical KS equations [29] and by the ETF density variational method using the profile (2.25) [27]. When including the 4th-order gradient terms in (2.18), the ETF solution agrees perfectly with the KS solution in the outer surface region, whereas the 2nd-order solution falls off too rapidly (as mentioned above). Note the shell oscillations in the quantum results.

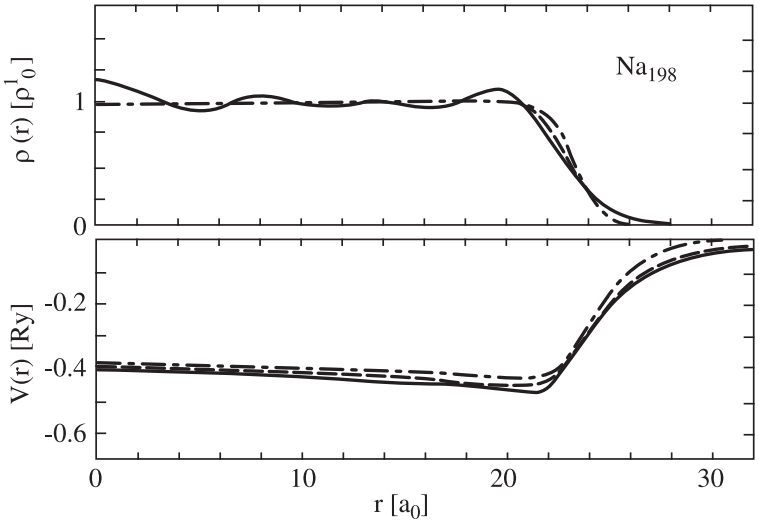

Fig. 2. Comparison of selfconsistent densities and potentials for the spherical Na_{198} cluster obtained in the jellium model. $V(r)$ is in Rydberg units, $\rho(r)$ in units of the ionic bulk density ρ_0^I. *Solid lines:* quantum-mechanical KS results [29]. *Dashed lines:* semiclassical ETF results including up to 4th-order gradient terms, and *dashed-dotted lines:* only up to 2nd-order gradient terms in the functional (2.18). (From [27].)

Fig. 3 shows a similar comparison for (a) the total energy per particle E/N and (b) the ionization potential IP for neutral spherical sodium clusters with N atoms obtained in the jellium model, plotted versus the cluster radius $R_I = r_s N^{1/3}$ (with a Wigner-Seitz radius of $r_s = 4$ a.u.). Again we see that the ETF results are smooth curves that miss the periodic shell effects but represents the correct average behaviour. The asymptotic limit of the IP for large clusters is the bulk work function W_b. Note that the electrostatic part of the IP shown at the bottom (c) oscillates much less than the other energies. The fact that the semiclassical total energy seems

to lie lower than the average of the quantum results is due to the imposed spherical symmetry. Indeed, the minima of the quantum results correspond the spherically "magic" clusters that have filled shells; in the regions in between, the clusters have only partially filled spherical shells and want to be deformed due to the Jahn-Teller effect. If a spontaneous symmetry breaking of the mean field is allowed in the KS calculation, their energies are systematically lowered, so that the ETF results come to lie much closer to the averaged KS results (see Ref. [31] and Sect. 3.5.2 for a discussion of the deformation effects).

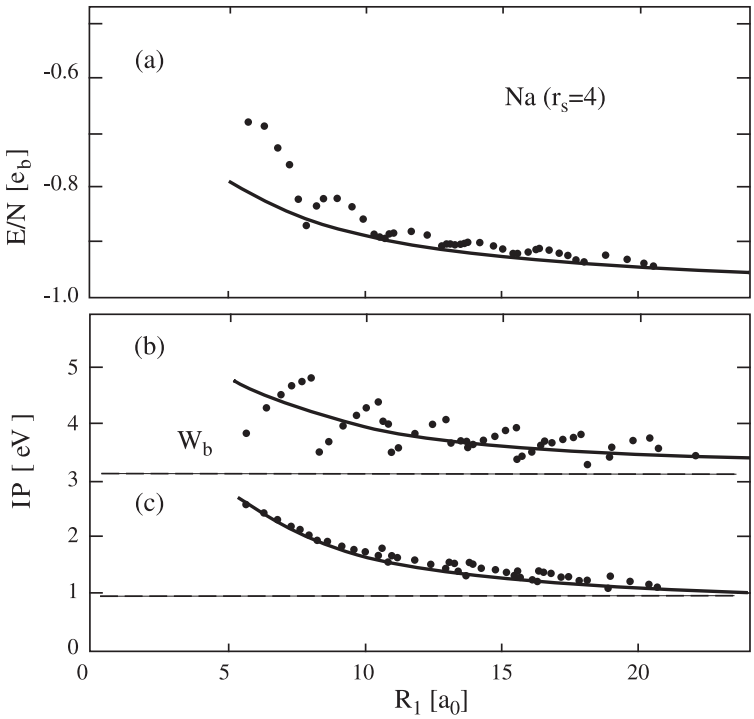

Fig. 3. *Upper part* (a): energies per atom E/N in units of the bulk value e_b; *lower part* (b): ionization potentials IP (in eV) for spherical jellium clusters with $r_s = 4$ a.u., shown versus cluster radius R_I. W_b is the bulk work function. Part (c) gives the electrostatic parts of the ionization potentials. Dots and small circles are the quantum-mechanical KS results [29]; the solid lines are the 4th-order ETF results [27]. (After [27].)

A comparison of experimental ionisation potentials IP and electron affinities EA [see their definitions in Eq. (2.27) below] of aluminum clusters with the variational ETF results [32], obtained in the spherical jellium model, is shown in Fig. 4 versus the inverse average cluster radius (which is proportional to $N^{1/3}$). The experimental results exhibit, of course, oscillations that come both from electronic shell effects and from the ionic structure that cannot be described by the jellium model. It is quite amazing that a simple semiclassical ETF calculation can capture the average experimental trends even down to the smallest molecules with $N = 3$, corresponding to the rightmost experimental point. [Note, however, that the calculated values have been vertically adjusted to fit the experimental bulk work function W_b at the intersection with the vertical axis, since the jellium model yields a wrong value of W_b. In this way, the average effects of the ionic structure has been taken into account implicitly (see [32] for details). See also Ref. [33] for improved results in the "stabilized" jellium model.]

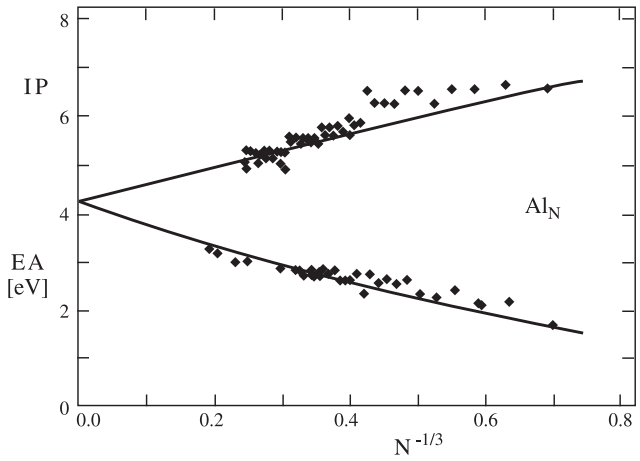

Fig. 4. Ionization potentials IP and electron affinities EA of aluminum clusters with N atoms, plotted versus the inverse cluster radius. *Black diamonds:* experimental results, *solid lines:* calculated ETF values in the spherical jellium model with $r_s = 2.99$. (From [32].)

2.5.2 Unrestricted spherical density variation

A test of the parametrization (2.25) of the spherical density profiles has been provided by unrestricted density variational calculations of Engel and Perdew [26] in the framework of the spherical jellium model. These authors solved numerically the Euler-Lagrange equation (2.22) including the

fourth-order gradient terms. Their density profiles $\rho(r)$, and quantities derived from them, are extremely well reproduced by the results of the restricted variation using the profiles (2.25). A similar test was done in nuclear physics [18] using the finite-temperature version of the ETF model. In Fig. 5 we show the density profiles $\rho(z)$ across the plane interface (positioned at $z = 0$) of nuclear matter in thermal equilibrium with a gas of nucleons, calculated for three different temperatures. The solid lines give the results obtained from the exact numerical solutions of the Euler-Lagrange variational equations (in one-dimensional planar geometry); the dashed lines are obtained using a restricted variation with the one-dimensional analogue of the parametrization (2.25).

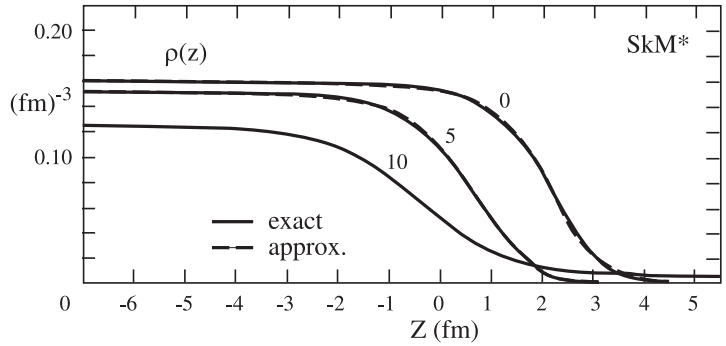

Fig. 5. Density profiles $\rho(z)$ for an interface of nuclear matter and a gas of nucleons in thermal equilibrium, calculated at the temperatures $T = 0$, 5, and 10 MeV. it Solid lines: exact solutions of the Euler-Lagrange equation (2.22) up to fourth order; *dashed lines:* results using a restricted parametrization of $\rho(z)$ corresponding to Eq. (2.25). (From [18].)

When the ionic structure is included in the theoretical description of metal clusters, the electronic density profiles can no longer be given by simple parametrizations, and unrestricted density variations become a necessity. This has been done by various groups [34–37] who performed variational (E)TF calculations for the electrons, in connection with molecular dynamics for the ions in the Born-Oppenheimer approach. As an example of the results of such calculations, we show in Fig. 6 the density profile of the highly deformed charged cluster Na_{18}^{++}, which has been called a "fission isomer" [35]. It has an approximate axial symmetry, and the density is shown here along the direction of the symmetry axis. The heavy line was obtained from solving the quantum-mechanical KS equations, whereas the thin line is obtained in the simple TF approximation.

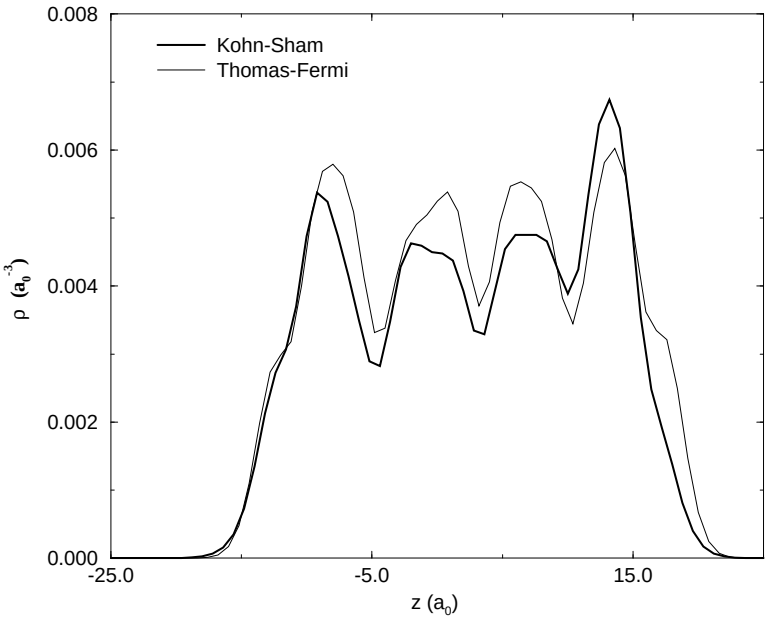

Fig. 6. Ground-state electron density $\rho(z)$ of the fission isomer of Na_{18}^{++}, computed quantum-mechanically in Kohn-Sham DFT (heavy line) and semiclassically in TF theory (thin line). (From [35].)

2.5.3 Liquid drop model for charged spherical metal clusters

We finally mention a useful application of ETF variational calculations to derive liquid-drop model (LDM) expansions of the total energy or other observables of a fermion system. When its density is of the form seen in Figs. 5 or 2 with a constant saturated value ρ_0 in the interior and a well-defined surface region a around the radius R where it falls off most steeply, one can perform analytically a so-called "leptodermous" expansion [19, 38] of all integrated quantities in powers of the small parameter a/R. For metal clusters this has been done systematically by Seidl [28, 39] within the spherical jellium model. The total energy of a cluster with N atoms and Z valence electrons is found to be:

$$\begin{aligned} E(N,Z) &= e_b N + a_s N^{2/3} + a_c N^{1/3} + a_0 - W_b(Z-N) \\ &+ \left\{ a_{-1} + \frac{e^2}{r_s}\left[C(Z-N) + \frac{1}{2}(Z-N)^2 \right] \right\} N^{-1/3} \\ &+ O(N^{-2/3})\,. \end{aligned} \tag{2.26}$$

For the ionization potential IP and the electron affinity EA, defined by

$$\mathrm{IP} = E(N,N-1) - E(N,N)\,, \quad \mathrm{EA} = E(N,N) - E(N,N+1)\,, \quad (2.27)$$

one finds the following expansions up to order $1/R = O(N^{-1/3})$:

$$\begin{aligned} \mathrm{IP}\,(R) &= W_b + \left(\frac{1}{2} - C\right)\frac{e^2}{R} + O(R^{-2})\,, \\ \mathrm{EA}\,(R) &= W_b - \left(\frac{1}{2} + C\right)\frac{e^2}{R} + O(R^{-2})\,. \end{aligned} \quad (2.28)$$

These expressions have been found to fit rather well the average experimental data for large clusters; the terms of order $O(R^{-2})$ become, however, particularly important for the electron affinities of small clusters [40] (see also Fig. 4 above).

All the parameters appearing in Eqs. (2.26,2.28) can be related to bulk properties (energy per particle e_b, Wigner-Seitz radius r_s) or properties of the infinite planar metal surface such as the work function W_b, the surface tension σ in $a_s = 4\pi r_s^2\sigma$, and other integrals [19,38] over the infinite surface density profile $\rho_\infty(x)$ (x being the distance from the plane with $x = 0$ at the jellium edge). In particular, the parameter C is given by

$$C = \frac{2}{3}\,\frac{a_s}{e^2/r_s} \;-\; 4\pi\int_0^\infty dx\,\Big[x^2\rho_\infty(x) + x f(x)\Big]\,, \quad (2.29)$$

where the function $f(x)$ appears in the asymptotic expansion of the density profile $\rho_R(r-R)$ of a large spherical cluster with radius R [26,33,41]:

$$\rho_R(x) = \rho_\infty(x) + \frac{f(x)}{R} + O(R^{-2})\,. \quad (2.30)$$

Note that C is *not* equal to 1/8, as was derived from a wrong classical image-potential argument which unfortunately still floats around in the literature and in the heads of some researchers. (See Ref. [42], where the flaw in this argument has been uncovered and corrected.) In fact, the quantity C, which in (2.28) above gives small deviations from the (correctly calculated) classical charging energy $e^2/2R$ of a sphere, is of purely quantum-mechanical origin with contributions from the kinetic and exchange-correlation energies of the electrons and the non-classical tail of their density.

The LDM expansion has also been discussed in the framework of the so-called "stabilized jellium model" [33] which yields improved bulk work functions and surface energies, and therefore provides a better starting point than the simple jellium model.

3 Periodic orbit theory for quantum shell effects

In this section, we shall describe the semiclassical approach to quantum shell effects. Historically, the "old" quantum theory by N. Bohr [43] started from a semiclassical approximation to the energy spectrum of the atom, requiring the action integral of the electron on its supposedly classical orbit around the nucleus to be an integer multiple of Planck's constant h (see Ref. [44] for a remarkable historical account). This semiclassical quantization scheme was later developed into the WKB method (named after Wenzel, Kramers and Brillouin [45]) for one-dimensional systems and, more than 30 years later, into the EBK quantization or "torus quantization" scheme for more-dimensional integrable systems. This method is named after Einstein, Brillouin, and Keller [46], who revived the idea of semiclassical quantization using the very fundamental observation by Einstein [47] that the classical motion of an integrable system is bound to a torus in phase space. (See, e.g., Ref. [4] for a presentation of the basic ideas of semiclassical quantization.)

The EBK method does not apply if a system with N degrees of freedom is not classically integrable, i.e., if it does not possess the same number N of constants of the motion which are independent and which Poisson-commute pairwise. The question if a non-integrable system can be quantized semiclassically remained therefore unanswered for some time. A break-through was accomplished by M. Gutzwiller [48], who derived a "trace formula" that connects the oscillating part of the quantum-mechanical level density to a sum over all periodic orbits of a classically non-integrable system. Independently, similar trace formulae were derived later by Balian and Bloch for particles in a cavity with reflecting walls (i.e., for three-dimensional billiards) [49], and by Berry and Tabor for integrable systems. Starting from EBK quantization, these authors first showed that the sum over the EBK spectrum can be converted quite generally in a sum over periodic orbits [50], and later derived the same result starting from Gutzwiller's semiclassical Green function [51] (see Sect. 3.1 below). Since the classical periodic orbits play a fundamental role in this semiclassical approach, it has been called "periodic orbit theory" (POT). Including a sufficient number of orbits in the trace formula, it can in principle yield the quantized energies of the system in the form of singularities (the peaks of the sum of delta functions). This works, however, only in a limited number of cases as the trace formulae represent asymptotic series which usually do not converge [52].

The applications of the POT which we want to discuss here do not aim at the quantization, but at a semiclassical description of *gross-shell* features in mean-field systems, which can be obtained by convoluting the level density with a smooth function over a finite energy range γ. Then, the periodic orbit sums converge [53] and only the orbits with the shortest periods and largest degeneracies become important.

We shall not derive here the trace formulae but refer to the original literature. For the approach of Gutzwiller, the reader may consult a monograph by the same author [52], and the very readable series of lectures which he presented a an earlier Les Houches Summer School [54]. The original trace formula of Gutzwiller [48] applies only to systems in which all orbits are isolated; this is the case for a classically chaotic system. A series of extensions to Gutzwiller's theory to take into account degenerate orbits, which appear in systems that possess continuous symmetries, have been developed over the past 30 years [55, 56]. Their basic ideas are discussed in Ref. [4].

In Sect. 3.1 we shall present the semiclassical Green function developed by Gutzwiller, which is the basic ingredient to all further developments in the POT. In Sect. 3.2 we present the trace formulae for the level density, particle number and total energy of a mean-field system, and in Sect. 3.3 we briefly discuss practical methods for finding periodic orbits and calculating their stabilities. Sect. 3.4 contains a summary of the problems connected with symmetry breaking transitions and orbit bifurcations, and indicates that these can be overcome by uniform approximations. The remaining parts are reserved for applications to metal clusters and mesoscopic semiconductor devices.

3.1 Semiclassical expansion of the Green function

The quantum-mechanical level density $g(E)$ given in Eq. (1.3) can be related to the imaginary part of the trace of the energy-dependent single-particle Green function $G(\mathbf{r}, \mathbf{r}'; E)$ for a system in D dimensions:

$$g(E) = -\frac{1}{\pi} \Im \int G(\mathbf{r}, \mathbf{r}; E + i\epsilon)\, d^D r\,. \qquad (\epsilon > 0) \tag{3.1}$$

The Green function itself is defined by

$$G(\mathbf{r}, \mathbf{r}'; E) = \sum_i \varphi_i^*(\mathbf{r}')\, \varphi_i(\mathbf{r})\, \frac{1}{(E - \varepsilon_i)} \tag{3.2}$$

and can be related to the single-particle propagator $K(\mathbf{r}, \mathbf{r}'; t)$ by a (half-sided) Fourier transform:

$$G(\mathbf{r}, \mathbf{r}'; E) = -\frac{i}{\hbar} \lim_{\epsilon \to 0} \int_0^\infty K(\mathbf{r}, \mathbf{r}'; t)\, \exp\left[\frac{i}{\hbar}(E + i\epsilon)t\right] dt\,. \tag{3.3}$$

Semiclassical approximations to the propagator go back to Van Vleck in 1928 [57]. Gutzwiller rederived Van Vleck's approximation from Feynman's path integral approach to quantum mechanics and improved it by the incorporation of some important phases. The basic idea of his derivation is the stationary phase approximation, applied to integrals containing a rapidly

oscillating phase. Doing also the Fourier transform in (3.3) by the stationary phase method, he arrived at the following semiclassical approximation to the Green function [48]:

$$G_{scl}(\mathbf{r},\mathbf{r}';E) \simeq \frac{2\pi}{(2\pi i\hbar)^{\frac{D+1}{2}}} \sum_{\alpha} \sqrt{|\mathcal{D}_\alpha|}\, \exp\left[\frac{i}{\hbar} S_\alpha(\mathbf{r},\mathbf{r}',E) - i\mu_\alpha \frac{\pi}{2}\right]. \quad (3.4)$$

The sum goes over all classical trajectories α that lead from the point $\mathbf{r}'$ to the point $\mathbf{r}$ at fixed energy E; the functions $S_\alpha(\mathbf{r},\mathbf{r}',E)$ are the action integrals along these trajectories:

$$S_\alpha(\mathbf{r},\mathbf{r}';E) = \int_{\mathbf{r}'}^{\mathbf{r}} \mathbf{p}''\cdot d\,\mathbf{r}'' = \sum_{i=1}^{D} \int_{r_i'}^{r_i} p_i(\mathbf{r}'',E)\, dr_i'' \,, \quad (3.5)$$

where r_i, p_i are the components of phase-space vectors $\mathbf{r}$ and $\mathbf{p}$, respectively. In Eq. (3.4), $\mathcal{D}_\alpha$ is the determinant of the $(D{+}1)$-dimensional matrix of second partial derivatives of the action integral with respect to all its arguments

$$\mathcal{D}_\alpha(\mathbf{r},\mathbf{r}';E) = \begin{vmatrix} \dfrac{\partial^2 S_\alpha}{\partial \mathbf{r}'\partial \mathbf{r}} & \dfrac{\partial^2 S_\alpha}{\partial \mathbf{r}'\partial E} \\[2ex] \dfrac{\partial^2 S_\alpha}{\partial E\partial \mathbf{r}} & \dfrac{\partial^2 S_\alpha}{\partial E^2} \end{vmatrix} . \quad (3.6)$$

The quantities μ_α in (3.4) count the number of caustic (or "conjugate") points along the trajectory α; they are connected to the Maslov indices appearing in the EBK quantization of integrable systems [46].

3.2 Trace formulae for level density and total energy

It remains only to insert the semiclassical Green function (3.4) into the relation (3.1) and to perform the trace integral. Taking $\mathbf{r}' = \mathbf{r}$ under the integral automatically selects only *closed* orbits from the sum over trajectories α. If these closed orbits are isolated in phase space, then all spatial integrals transverse to the orbits can again be done using the stationary phase approximation; only the integration along the orbit is done exactly. The stationary condition for the exponent in (3.4) leads, using Eq. (3.5), to

$$\left[\frac{\partial S}{\partial \mathbf{r}}\right]_{\mathbf{r}_0} = \left[\frac{\partial S(\mathbf{r},\mathbf{r}',E)}{\partial \mathbf{r}} + \frac{\partial S(\mathbf{r},\mathbf{r}',E)}{\partial \mathbf{r}'}\right]_{\mathbf{r}'=\mathbf{r}=\mathbf{r}_0} = \mathbf{p}-\mathbf{p}' = 0\,, \quad (3.7)$$

where $\mathbf{r}_0$ is the point where S becomes stationary. Eq. (3.7) implies that the orbits are not only closed but *periodic*, i.e., they have to start and end with the same momentum: $\mathbf{p}' = \mathbf{p}$. The transformation to a coordinate

system co-moving with each periodic orbit, the evaluation of the saddle-point integrations, and expressing the result in a canonically invariant form – all this requires quite some tedious algebra and finally leads to Gutzwiller's famous trace formula for isolated orbits [48]:

$$\delta g_{scl}(E) \simeq \frac{1}{\hbar\pi} \sum_{po} \frac{T_{ppo}}{\sqrt{|\det\left(\widetilde{\mathbf{M}}_{po} - \mathbf{1}\right)|}} \cos\left(\frac{1}{\hbar} S_{po} - \sigma_{po} \frac{\pi}{2}\right). \tag{3.8}$$

The sum here goes over all periodic orbits *po*, including their repeated cycles. $\widetilde{\mathbf{M}}_{po}$ is the stability matrix discussed in Sect. 3.3 below and $\mathbf{1}$ the unit matrix with the same dimension, S_{po} is the action integral along the (repeated) periodic orbit

$$S_{po}(E) = \oint_{po} \mathbf{p} \cdot d\mathbf{r}\,, \tag{3.9}$$

$T_{ppo} = \partial S_{ppo}/\partial E$ is the period of the *primitive* periodic orbit (i.e., its first cycle), and σ_{po} is the so-called Maslov index which arises as a sum of the phase index μ_{po} occurring in the semiclassical Green function (3.4) plus an index ν_{po} (being 1 or 0 for a two-dimensional system) that stems from the stationary-phase evaluation of the trace integral. (See also Ref. [58], where it has been shown that the total Maslov index $\sigma_{po} = \mu_{po} + \nu_{po}$ is a canonical and topological invariant, whereas μ_{po} and ν_{po} alone may depend on the starting point along the orbit or on the choice of the coordinate system.) The index σ_{po} may also be obtained as a winding number [58,59]. All quantities appearing on the r.h.s. of the trace formula (3.8) depend smoothly on the energy E. (The Maslov indices are integer constants in finite energy intervals but usually change abruptly by one or more units at bifurcations; see Sect. 3.4 below.)

For systems that contain continuous symmetries, most (or all) periodic orbits are not isolated in phase space but appear in degenerate families. The single orbits within these families can be smoothly transformed into each other by a symmetry operation (translation, rotation, etc.) that does not affect their properties (actions, stabilities, Maslov indices). Consequently, the stationary-phase approximation to some of the trace integrations perpendicular to the orbits breaks down (namely the directions in which the orbits can be displaced by these symmetry operations and in which the actions remain constant). As a result, the determinant in the denominator of (3.8) becomes zero and the trace formula diverges. Similar problems arise also in isolated situations (e.g., at specific energies or values of some other continuous system parameter) in connection with orbit bifurcations and symmetry-breaking (or symmetry-restoring) transitions. For these latter situations special uniform approximations can be developed, which will be briefly discussed in Sect. 3.4.

The problem of continuous orbit degeneracies can be solved by performing *exactly* the trace integrations in those directions where the action remains constant [55, 56]. (See Ref. [4] for a detailed discussion of different techniques used hereby.) The results of these extensions of the Gutzwiller theory are trace formulae of the general form, which also applies to those derived earlier for billiards [49] and integrable systems [50, 51]:

$$\delta g_{scl}(E) \simeq \sum_{po} \mathcal{A}_{po}(E) \cos\left[\frac{1}{\hbar} S_{po}(E) + \sigma_{po}\frac{\pi}{2}\right]. \tag{3.10}$$

Here the sum goes over all distinct periodic orbit families (plus isolated orbits if they exist). The overall Maslov indices σ_{po} may also become half-integer. The precise form of the amplitudes $\mathcal{A}_{po}$ depends on the particular symmetry of the system. The inverse power of $\hbar$ contained in these amplitudes equals $1+f/2$ where f is the degree of degeneracy of a given orbit family, i.e., the number of independent continuous parameters describing its degeneracy (or, equivalently, the number of different symmetry operations possible, or the dimension of the group creating these symmetry operations). Note that families with different degrees of degeneracy and isolated orbits with $f = 0$ may coexist in one and the same system. For example, in a three-dimensional system with spherical symmetry, the most degenerate orbit families occur with a three-fold continuous degeneracy ($f = 3$), because their possible orientations are described by the three Euler angles; the group creating the corresponding rotations is the SO(3) group; the amplitudes $\mathcal{A}$ of these orbits are proportional to $\hbar^{-5/2}$. In a spherical billiard, there is also the linear orbit bouncing along a diameter; its degeneracy is only $f = 2$ since rotation about its own direction does not create a new orbit. If the potential is a smooth and attractive central field $V(r)$, there exists also an isolated orbit with $f = 0$, namely the circular orbit with a radius corresponding to the minimum of the effective potential $V(r) + L^2/2mr^2$ for a given non-zero angular momentum L.

When applying the POT to a fermionic mean-field system, one is also interested in integrated quantities obtained from the level density. Its first integral gives the number of particles, see Eq. (2.3). Performing the energy integration in the saddle-point approximation yields the trace formula for the oscillating part of the function $N(E_F)$:

$$\delta N_{scl}(E_F) \simeq \sum_{po} \left(\frac{\hbar}{T_{po}}\right) \mathcal{A}_{po}(E_F) \sin\left[\frac{1}{\hbar} S_{po}(E_F) + \sigma_{po}\frac{\pi}{2}\right], \tag{3.11}$$

where T_{po} is the period of the (repeated) periodic orbit (family) at the Fermi energy E_F. The oscillating part δE of the total binding energy of an interacting system in the mean-field approximation can be shown [2, 55] to

be given, to leading order in the oscillating part of the level density δg, by

$$\begin{aligned} \delta E_{scl} &\simeq \int_0^{E_F} (E - E_F)\, \delta g(E)\, dE \\ &\simeq \sum_{po} \left(\frac{\hbar}{T_{po}}\right)^2 \mathcal{A}_{po}(E_F)\, \cos\left[\frac{1}{\hbar} S_{po}(E_F) + \sigma_{po}\frac{\pi}{2}\right]. \end{aligned} \tag{3.12}$$

(See also Ref. [4] for a discussion of the "Strutinsky theorem" from which the first equation above can be derived.) Note that in the above two trace formulae, only the orbit properties at the Fermi energy E_F are required.

In most realistic physical systems, the periodic orbits and their properties can only be calculated numerically (see Sect. 3.3) – which, as already mentioned, can be a very difficult task. For systems which are only weakly perturbed away from an analytically known integrable limit, a perturbative trace formula has been developed by Creagh [60], for which the perturbed orbits need not be determined. Assume a Hamiltonian of the form

$$\hat{H} = \hat{H}_0 + \epsilon \hat{H}_1\,, \tag{3.13}$$

where $\hat{H}_0$ is integrable and ϵ is a small dimensionless number. The idea now is that to lowest order in ϵ, the amplitudes and Maslov indices in the trace formula will not be affected by the perturbation, and that only the lowest-order change δS_{po} induced by $\epsilon \hat{H}_1$ has to be retained in the phase. The perturbed trace formula is then of the form

$$\delta g_{scl}\,(E) \simeq \Re\left\{\sum_{po} \mathcal{A}_{po}^{(0)}(E)\, \mathcal{M}_{po}(x) e^{i\left[\frac{1}{\hbar} S_{po}^{(0)}(E) + \sigma_{po}^{(0)}\frac{\pi}{2}\right]}\right\}, \tag{3.14}$$

where the quantities with superscript "(0)" are those appearing in the trace formula for the unperturbed system $\hat{H}_0$, and $\mathcal{M}_{po}(x)$ is a – generally complex – modulation factor defined as the average of the phase change due to δS_{po} over the unperturbed orbit family:

$$\mathcal{M}_{po}(x) = \langle e^{i\delta S_{po}/\hbar} \rangle_{po}\,. \tag{3.15}$$

The argument x of the modulation factor is proportional to the lowest power of ϵ for which the action change δS_{po} is non-zero, inverse proportional to $\hbar$, and further depends on the energy E. The perturbative trace formula for the total energy is correspondingly given by

$$\delta E_{scl} \simeq \Re\left\{\sum_{po} \mathcal{A}_{po}^{(0)}(E_F)\, \mathcal{M}_{po}(x) \left(\frac{\hbar}{T_{po}}\right)^2 e^{i\left[\frac{1}{\hbar} S_{po}^{(0)}(E_F) + \sigma_{po}^{(0)}\frac{\pi}{2}\right]}\right\}. \tag{3.16}$$

By construction, the unperturbed trace formulae are recovered in the limit $\epsilon \to 0$. For large values of ϵ, this approach will eventually break down and

uniform approximations must be used to recover the correct amplitudes of the trace formula applying to the strongly perturbed system (see Sect. 3.4).

All the above trace formulae are remarkable in the sense that they relate the quantum-mechanical oscillations contained in their left-hand side with a sum over periodic orbits on their right-hand side that includes only properties of the classical system. They represent asymptotic series which can be expected to become exact in the limit $S_{po} \gg \hbar$. As already mentioned in the introduction to this section, these series usually do not converge, and in many systems the problem of enumerating all periodic orbits and calculating their properties is practically not solvable. There exist a few soluble (integrable and non-integrable) systems for which the trace formula can be shown to converge to a sum of delta functions if the smooth part $\widetilde{g}(E)$ of the level density is added to it – and for a few of those, the result is even identical to the exact quantum-mechanical level density [4, 52]. But these are rare exceptions.

For the applications discussed here, both sides of the trace formulae are convoluted with a normalized Gaussian function $\exp\left[-(E/\gamma)^2\right]/\sqrt{\pi}\gamma$. Using saddle-point integration for the convolution of the periodic orbit sum, one obtains an extra factor

$$\exp\left[-\left(\frac{\gamma}{2}\frac{T_{po}}{\hbar}\right)^2\right] \tag{3.17}$$

under the summations in all trace formulae above. This factor suppresses the orbits with longer periods and usually leads to the convergence of the orbit sums (cf. Ref. [53]). In particular, it shows that the *gross-shell* effects are governed by the shortest orbits. Exact quantization by summing over all orbits can still be attempted by taking the limit $\gamma \to 0$.

Concerning the smooth part $\widetilde{g}(E)$ of the level density that was the subject of Sect. 2, it has been shown [49, 61] to arise within the periodic orbit theory from the closed orbits of *zero length* (and hence zero action) that mathematically also contribute to the sum of trajectories in the semiclassical Green function (3.4) when taking the trace integral in (3.1). Since their actions (and also their Maslov indices) are zero, they do not contribute in an oscillatory fashion to the level density but just constitute its phase-space average which yields the (extended) TF approximation as discussed in Sect. 2. This becomes particularly transparent in the derivation of the trace formula for integrable systems by Berry and Tabor [50] (see Ref. [4] for some exactly soluble models).

3.3 Calculation of periodic orbits and their stability

We briefly present here the linear stability analysis of periodic orbits and how the stability matrix can be used to find periodic orbits. We start from

a holonomic Hamiltonian with a local potential $V(\mathbf{r})$ in D dimensions:

$$H(\mathbf{r},\mathbf{p}) = \frac{1}{2}\,\mathbf{p}^2 + V(\mathbf{r})\,. \tag{3.18}$$

(We put the mass equal to unity and assume the kinetic energy to be quadratic in $\mathbf{p}$ just for simplicity of the presentation here; any general dependence of $\mathbf{p}$ and $\mathbf{r}$ is allowed in principle.) Hamilton's equations of motion

$$\dot{\mathbf{p}} = -\frac{\partial H}{\partial \mathbf{r}}\,, \qquad \dot{\mathbf{r}} = \frac{\partial H}{\partial \mathbf{p}} \tag{3.19}$$

are in general non-linear. Assume now that we have found a periodic orbit, i.e., a T-periodic solution

$$\mathbf{r}_0(t) = \mathbf{r}_0(t+T)\,, \qquad \mathbf{p}_0(t) = \mathbf{p}_0(t+T)\,, \tag{3.20}$$

and that $V(\mathbf{r})$ in Eq. (3.18) is holomorphic around $V(\mathbf{r}_0)$. (We shall turn further below to the question how to find such a periodic orbit practically.) We now want to investigate the stability of this solution with respect to some small perturbations $\delta\mathbf{r}$, $\delta\mathbf{p}$:

$$\mathbf{r} = \mathbf{r}_0 + \delta\mathbf{r}\,, \qquad \mathbf{p} = \mathbf{p}_0 + \delta\mathbf{p}\,. \tag{3.21}$$

Substituting (3.21) into (3.19) and expanding up to second order with respect to the perturbations, we find the $2D$ *linearized* differential equations for $\delta\mathbf{r}$ and $\delta\mathbf{p}$, also called the Poincaré variational equations:

$$\frac{d}{dt}\begin{pmatrix} \delta\mathbf{r} \\ \delta\mathbf{p} \end{pmatrix} = \begin{pmatrix} \mathbf{0} & \mathbf{1} \\ -\mathbf{V''}_0(t) & \mathbf{0} \end{pmatrix}\begin{pmatrix} \delta\mathbf{r} \\ \delta\mathbf{p} \end{pmatrix}, \tag{3.22}$$

where $\mathbf{0}$ and $\mathbf{1}$ are the D-dimensional zero and unit matrices, respectively, and $\mathbf{V''}_0(t)$ is the matrix of second derivatives of the potential $V(\mathbf{r})$, taken at $\mathbf{r}_0(t)$:

$$(\mathbf{V''}_0)_{ij}(t) = \left.\frac{\partial^2 V(\mathbf{r})}{\partial r_i \partial r_j}\right|_{\mathbf{r}=\mathbf{r}_0(t)}\,. \qquad (i,j=1,2,\ldots,D) \tag{3.23}$$

Eq. (3.22) is a set of linear differential equations with T-periodic coefficients. From their general theory (see, e.g., Ref. [62]) one learns that the evolution of some initial perturbation $\delta\mathbf{r}$, $\delta\mathbf{p}$ at time $t=0$ up to the time t is given by

$$\begin{pmatrix} \delta\mathbf{r}(t) \\ \delta\mathbf{p}(t) \end{pmatrix} \;=\; \mathbf{X}(t)\begin{pmatrix} \delta\mathbf{r}(0) \\ \delta\mathbf{p}(0) \end{pmatrix}, \tag{3.24}$$

where $\mathbf{X}(t)$ is the so-called "matrizant" of dimension $2D$. From Eq. (3.22) it is seen that the matrizant fulfills the differential equation

$$\frac{d}{dt}\,\mathbf{X}(t) \;=\; \begin{pmatrix} \mathbf{0} & \mathbf{1} \\ -\mathbf{V''}_0(t) & \mathbf{0} \end{pmatrix}\mathbf{X}(t) \tag{3.25}$$

with the initial conditions

$$(\mathbf{X})_{mn}(0) = \delta_{mn}\,. \qquad (m,n = 1,2,\ldots,2D) \tag{3.26}$$

The value of the matrix $\mathbf{X}(t)$ at the time of the period T is called the "monodromy matrix" $\mathbf{M}$:

$$\mathbf{M} = \mathbf{X}(T)\,. \tag{3.27}$$

$\mathbf{M}$ is a symplectic $(2D \times 2D)$ matrix. According to the Lyapounov-Poincaré theorem, its eigenvalues λ_m $(m = 1,2,\ldots,2D)$ are pairwise inverse. Furthermore, two of the eigenvalues are always equal to unity, corresponding to small perturbations that either occur along the orbit or amount to a rescaling of the energy. Thus, $\mathbf{M}$ can always be brought into the form

$$\mathbf{M} = \begin{pmatrix} \widetilde{\mathbf{M}} & \begin{matrix} \cdots \end{matrix} \\ \mathbf{0} & \begin{pmatrix} 1 & \cdots \\ 0 & 1 \end{pmatrix} \end{pmatrix}, \tag{3.28}$$

where the $2D-2$ dimensional submatrix $\widetilde{\mathbf{M}}$ is the stability matrix appearing in the denominator of Gutzwiller's trace formula (3.8). The stability matrix thus describes the propagation of a small perturbation $(\mathbf{r}_\perp, \mathbf{p}_\perp)$, transverse (in phase space) to the given periodic orbit, over one period T:

$$\begin{pmatrix} \delta\mathbf{r}_\perp(T) \\ \delta\mathbf{p}_\perp(T) \end{pmatrix} = \widetilde{\mathbf{M}} \begin{pmatrix} \delta\mathbf{r}_\perp(0) \\ \delta\mathbf{p}_\perp(0) \end{pmatrix}. \tag{3.29}$$

Its eigenvalues give us the information on the stability of the periodic orbit. Note that $\det \widetilde{\mathbf{M}} = 1$, which expresses the fact that the Poincaré mapping defined by Eq. (3.29) is area preserving.

For two-dimensional systems ($D = 2$), the stability matrix is also two-dimensional and the stability analysis becomes particularly simple. Its two eigenvalues are just λ and $1/\lambda$, so that

$$\mathrm{tr}\,\widetilde{\mathbf{M}} = \lambda + 1/\lambda\,. \qquad (D = 2) \tag{3.30}$$

For *stable* orbits, the eigenvalues lie on the complex unit circle, so that $\lambda = e^{\pm i\kappa}$ and a small perturbation just keeps oscillating around the periodic orbit. The real number κ is called the stability angle. For *unstable* orbits, the eigenvalues are of the form $\lambda = \pm e^{\pm\chi}$, where the real $\chi > 1$ is the Lyapounov exponent which measures the rate at which a small initial perturbation is growing exponentially in magnitude. Actually, one does not need to compute the eigenvalues of $\widetilde{\mathbf{M}}$ to find out if an orbit is stable or not: since, as is easily seen from the above, $|\mathrm{tr}\,\widetilde{\mathbf{M}}| > 2$ for unstable and $|\mathrm{tr}\,\widetilde{\mathbf{M}}| < 2$ for stable orbits, it is enough to know the trace of $\widetilde{\mathbf{M}}$. When $|\mathrm{tr}\,\widetilde{\mathbf{M}}| = 2$, an orbit is called *neutrally stable* or *marginally stable*; this is

the case for all families of degenerate orbits occurring in (integrable) systems with continuous symmetries. It is easily seen that the quantity under the root in the denominator of the trace formula (3.8) for $D = 2$ becomes $|\det(\widetilde{\mathbf{M}}_{po} - \mathbf{1})| = |2 - \mathrm{tr}\,\widetilde{\mathbf{M}}|$, so that the formula diverges for all contributions from marginally stable orbit families. The other situation where the same divergence occurs is, as already mentioned in Sect. 3.2, when $\mathrm{tr}\,\widetilde{\mathbf{M}} = +2$ for an isolated orbit. This happens in connection with orbit bifurcations which we will discuss briefly in Sect. 3.4.

Using the stability matrix we can now give a practical recipe for finding periodic orbits of a Hamiltonian system. The idea is to exploit Eq. (3.29) for a Newton-Raphson iteration procedure (see, e.g., Ref. [59]). For this, we have to calculate the stability matrix during our search for periodic orbits. This is done by solving simultaneously the Hamilton equations of motion (3.19) *and* the equation of motion for the matrizant $\mathbf{X}(t)$ given in Eq. (3.25). [Actually, to get rid of the two irrelevant degrees of freedom along the orbit, one may transform immediately to the coordinates $\mathbf{r}_\perp$, $\mathbf{p}_\perp$ orthogonal to the orbit, to obtain the reduced part $\widetilde{\mathbf{X}}(t)$ which after one period T gives $\widetilde{\mathbf{M}} = \widetilde{\mathbf{X}}(T)$; see Ref. [59] for the equations of motion for $\widetilde{\mathbf{X}}(t)$.]

Let us introduce a short notation $\mathbf{z} = (\mathbf{r}_\perp, \mathbf{p}_\perp)$ for the orthogonal phase-space vector. Usually, the search of periodic orbits is done on a Poincaré surface of section, on which small displacements are automatically transverse to the searched orbit. We now assume that we have found an approximate periodic solution with the approximate period T. If we are close enough to the fixed point $\mathbf{z}^*$ corresponding to the exact periodic solution, the remaining error of our approximate first starting point $\mathbf{z}_1$ will propagate according to Eq. (3.29). After one period, the starting point $\mathbf{z}_1$ is mapped onto $\mathbf{z}_1'$, so that we have moved over an interval $\Delta\mathbf{z}_1 = \mathbf{z}_1' - \mathbf{z}_1$. The distances of the two points from the unknown fixed point $\mathbf{z}^*$ are $\delta\mathbf{z}_1 = \mathbf{z}_1 - \mathbf{z}^*$ and $\delta\mathbf{z}_1' = \mathbf{z}_1' - \mathbf{z}^*$. If $\delta\mathbf{z}_1$ and $\delta\mathbf{z}_1'$ are sufficiently small, they obey the linear differential equation (3.29), so that

$$\delta\mathbf{z}_1' = \widetilde{\mathbf{M}}\,\delta\mathbf{z}_1\,, \tag{3.31}$$

from which we get, using $\Delta\mathbf{z}_1 = \delta\mathbf{z}_1' - \delta\mathbf{z}_1$,

$$\Delta\mathbf{z}_1 = (\widetilde{\mathbf{M}} - \mathbf{1})\,\delta\mathbf{z}_1\,. \tag{3.32}$$

This equation can be inverted to obtain the error $\delta\mathbf{z}_1$ of our starting point

$$\delta\mathbf{z}_1 = (\widetilde{\mathbf{M}} - \mathbf{1})^{-1}\Delta\mathbf{z}_1, \tag{3.33}$$

which now can be used to correct the starting point to $\mathbf{z}_2 = \mathbf{z}_1 - \delta\mathbf{z}_1$. Iterating in this way, the fixed point is usually found within very few steps. The only problem with this procedure is that for an orbit with two eigenvalues

$\lambda = 1$, the inversion of $(\widetilde{\mathbf{M}} - \mathbf{1})$ is not possible, giving exactly the same divergence that appears in the trace formula (3.8). In practice, this is not a big handicap; when working with a sufficient numerical accuracy, one can come sufficiently close to the point where $\mathrm{tr}\,\widetilde{\mathbf{M}} = 2$.

The Newton-Raphson iteration converges very fast, once one comes close enough to a periodic orbit (i.e., a fixed point). It is therefore possible to search periodic orbits just by scanning a given Poincaré surface of section, either systematically in small steps, or just randomly. The practical experience shows that, different from what one might expect at first thought, stable and unstable fixed points are found with equal probability.

3.4 Uniform approximations

A classical system that is neither integrable nor fully chaotic is usually called a "mixed system", or a system with mixed classical dynamics. It is characteristic of such systems that periodic orbits change their stability upon variation of a smooth parameter. Such a parameter may be the energy, any parameter appearing in the potential $V(\mathbf{r})$ (e.g., a deformation parameter), or the strength of an externally applied electric or magnetic field. Let us call this parameter a. Whenever a pair of eigenvalues of the stability matrix for a periodic orbit has the value $\lambda = 1$ (i.e., $\mathrm{tr}\,\widetilde{\mathbf{M}} = 2$ for a two-dimensional system) at $a = a_0$, then the orbit undergoes a bifurcation. What typically happens at a bifurcation is that an orbit changes from stable to unstable (or *vice versa*), and hereby one or several new orbits are "born". (Orbits may also just "touch" the value $\mathrm{tr}\,\widetilde{\mathbf{M}} = 2$ at $a = a_0$ without changing their stability, or a pair of stable and unstable orbits may emerge for $a \geq a_0$ and not exist at all for $a < a_0$.) Infinitesimally close to the bifurcation point a_0, the new "child" orbits have the same shape and action as the "parent" orbit (but usually a different Maslov index). As one changes a away from a_0, the new orbits develop independently, and eventually change their stability again at a new bifurcation point a_1. Often, periodic orbits proliferate this way in chains of repeated bifurcations, leading to an increased degree of chaoticity (cf. the so-called Feigenbaum scenario [63, 64] and Ref. [65]).

This behaviour of periodic orbits in mixed systems makes the semiclassical POT difficult, since the trace formulae diverge at each bifurcation point. Mathematically speaking, the divergence comes from the fact that one of the stationary phase integrations used in their derivation (see Sect. 3.2) breaks down. The remedy is, in principle, to expand the action integral in the exponent of the semiclassical Green function (3.4) up to higher order and then to do the corresponding integration. For instance, when integrating along a direction x, one may have to expand the exponent up to third order in $(x - x_0)$, where x_0 is the stationary point; the integral over x then would lead to an Airy function. More generally, one expands the action integral

around the stationary point $\mathbf{r}_0$, $\mathbf{p}_0$ in phase space (corresponding to the bifurcation point a_0) into so-called normal forms [66] and then performs the trace integrations (if possible, analytically). This locally removes the singularity at $a = a_0$, but it does not yet guarantee that the result can be used further away: when a is sufficiently different from a_0 one wants to recover the original Gutzwiller amplitudes $\mathcal{A}_{po}$. To guarantee this, more refined techniques are required, yielding so-called "uniform approximations". Such approximations have been developed systematically for all generic types of orbit bifurcations by Sieber and Schomerus [67], and for pairs of interfering bifurcations by Schomerus [68]. We refer to their articles for further details; the resulting trace formulae have finite amplitudes at the bifurcation points and go over into the standard Gutzwiller trace formula away from the bifurcations.

Uniform approximations are also required when the change of a smooth parameter, or its being switched from zero to non-zero (or *vice versa*) leads to the breaking (or restoring) of a continuous symmetry. As we have discussed in Sect. 3.2 after Eq. (3.10), the power of $\hbar$ contained in the Gutzwiller amplitude $\mathcal{A}_{po}$ depends on the number f of continuous symmetry parameters describing the degeneracy of orbit families. When f is changed by one or more units upon variation of a parameter, the original form of the amplitude becomes invalid and therefore diverges. Start, e.g., from a two-dimensional billiard with oval boundary, which is non-integrable (with $f = 0$) so that the Gutzwiller trace formula (3.8) applies. Now, when letting its shape go to a circle, $\mathrm{tr}\,\widetilde{\mathbf{M}}$ of all the isolated periodic orbits will approach the value $+2$. Thus the trace formula diverges in the limit where the circular U(1) symmetry is restored and the billiard becomes integrable (with $f = 1$). (The amplitudes there are all proportional to $\hbar^{-3/2}$.)

Such a symmetry breaking arises generically if we perturb an integrable Hamiltonian like in Eq. (3.13) by switching on the parameter ϵ. For small values of ϵ, the perturbative trace formula (3.14) solves this problem but, as already mentioned, for large values ϵ its amplitudes do not go over to the correct Gutzwiller amplitudes of the perturbed system. The techniques used to achieve this are similar to those used to derive the uniform approximations for bifurcations. For the breaking of U(1) symmetry, a general uniform approximation has been derived by Tomsovic *et al.* [69], and uniform approximations for SU(2) and SO(3) breaking have been derived for some specific systems in Ref. [70].

Finally, we mention that in Ref. [71] an analytical trace formula has been given for the two-dimensional elliptic billiard in which – although it is integrable! – an infinity of bifurcations occur that cumulate in the limit of zero eccentricity (i.e., the circular billiard), so that both bifurcations and symmetry breaking had to be overcome.

3.5 Applications to metal clusters

The examples given here for metal clusters will be short, since they have already been discussed extensively at various occasions [4, 31, 72].

3.5.1 Supershell structure of spherical alkali clusters

Based upon the semiclassical trace formula derived by Balian and Bloch [49] for the oscillating level density of a spherical billiard, and extending the semiclassical POT analysis to Woods-Saxon type shell-model potentials for large clusters, Nishioka *et al.* [73] predicted that supershell structure should be experimentally observable in large metal clusters. This was, indeed, verified in the experiments of the Copenhagen-Stuttgart collaboration [74]. Fig. 7 shows the oscillating part of the cluster abundance in an adiabatic expansion source. Shown are the statistically averaged fist differences of the logarithmic yields I_N, multiplied by a factor that accounts for the temperature suppression effects (see Refs. [30, 75] for a theoretical investigation of these effects in finite-temperature Kohn-Sham calculations for canonical ensembles of spherical jellium clusters).

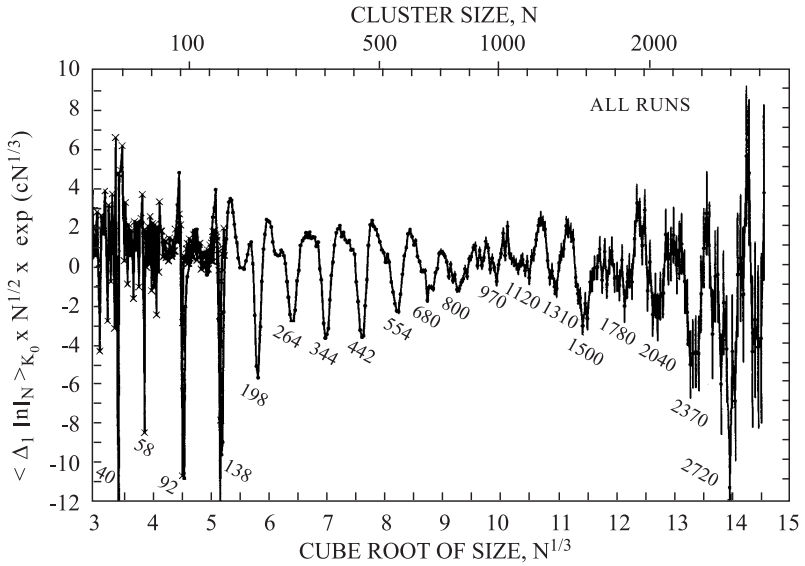

Fig. 7. Experimental observation of the supershells. Shown are the logarithmically derived relative yields of sodium clusters from an adiabatic expansion source, scaled by an extra factor $N^{1/2}\exp(cN^{1/3})$ that takes account of the finite temperature effects. (After [74].)

The negative peaks in Fig. 7 correspond to the most stable clusters which are understood as those with filled spherical *electronic* shells with the "magic numbers" indicated. Note that they appear at equal distances on the scale $N^{1/3}$ which is proportional to the cluster radius. The constant spacing $s = \Delta N^{1/3}$ is experimentally found to be $s = 0.61 \pm 0.01$, also for other metal clusters (Li, Ga). The beating amplitude of the shell oscillations is understood in the POT from the interference of the shortest periodic orbits with largest amplitude, which here are the triangular and square orbits. Their *average length* determines the shell spacing s; from the trace formula of a spherical billiard [49] one finds the value $s = 0.603$ which is independent of the Wigner-Seitz parameter r_s of the metal. The calculations of Nishioka *et al.* yield $s = 0.607$; the same value is found in the jellium-model DFT calculations for spherical Na clusters [30]. (Some finer details in connection with the Ga experiments are discussed in Ref. [76].) The beat length, i.e., the period of the supershells, is given essentially by the *difference* between the lengths of the leading orbits. It does depend on the metal type (see a detailed investigation in Ref. [77]).

The effect of a magnetic field on the supershell structure was investigated semiclassically with the perturbative trace formula of Eq. (3.14) in Ref. [78]. The field strengths necessary to detect interesting effects are, however, not experimentally available. (This is different for the mesoscopic sizes of quantum dots, as discussed further below.)

3.5.2 Ground-state deformations

As we know from nuclei, finite fermion systems may become deformed if a spherical shell is not completely filled: in order to avoid the degeneracy of the wavefunction, the system responds by a spontaneous breaking of the spherical symmetry. In molecular physics, this corresponds to the well-known Jahn-Teller effect. In the pioneering experiments on sodium clusters by the group of Walter Knight [79,80], the finer structures in the mass yields between the spherically magic numbers were, indeed, understood in terms of a deformed shell model (see Ref. [40] for details). Most of the smaller minima appearing in Fig. 7 for cluster sizes up to $N \sim 800$ could, in fact, also be attributed to deformed cluster shapes [81].

The POT analysis for deformed potentials becomes more complicated, as these usually are not integrable. Simple estimates of cluster deformations are, however, possible in terms of integrable deformed model potentials. This has been done successfully in nuclear physics by Strutinsky *et al.* [55]. Assume that only one periodic orbit, or one family of periodic orbits, is dominating the shell-correction energy δE given by (3.12). The condition for finding its extrema then reduces to

$$\delta S_{po} = 0\,. \tag{3.34}$$

This idea has been used for metal clusters in Ref. [82]. Fig. 8 compares semiclassical estimates of the ground-state quadrupole deformations δ with results of quantum-mechanical calculations. For small clusters up to $N \sim 40$, the selfconsistent Kohn-Sham field is well approximated by an axially deformed harmonic oscillator whose exact trace formula is known analytically [83]. In the limit of large clusters, the mean field has very steep walls, as demonstrated by the success of the spherical billiard model for the supershells. For large deformed clusters it may therefore be approximated by a spheroidal billiard, whose approximate trace formula is also known analytically [84]. The heavy lines in Fig. 8 give the semiclassical estimates of δ using these exact trace formulae and Eq. (3.34). The thin lines are the quantum-mechanical results from KS calculations in the deformed jellium model [85] for $N \leq 40$, and for $N > 40$ from calculations using Strutinsky's shell-correction method [2] in a phenomenological modified Nilsson model for large clusters that yields the spherical KS spectra [81].

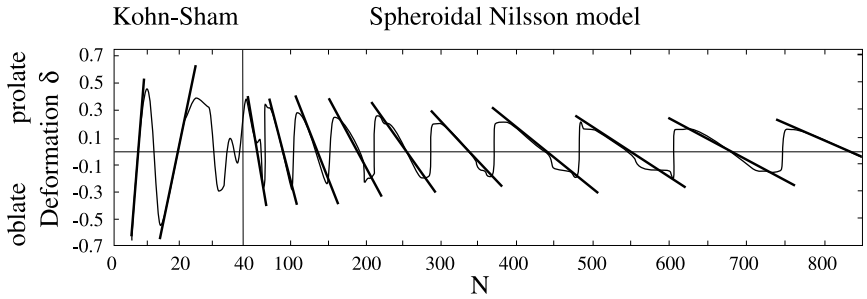

Fig. 8. Ground-state quadrupole deformations δ of sodium clusters versus cluster size N. The solid thin lines for $N \leq 40$ are the results from KS calculations using the spheroidal jellium model [85], and for $N > 40$ those from microscopic Strutinsky calculations using a modified Nilsson model that is adjusted to the spherical jellium-KS results [81]. The heavy lines give the semiclassical estimates based on Eq. (3.34) using the trace formula of an axial harmonic oscillator for $N < 26$ and that of a spheroidal billiard for $N > 40$. (From [82].)

More realistic deformed potentials have mixed classical dynamics, which leads to the problems discussed in Sect. 3.4 above. The POT analysis then depends on finding the most important short orbits and treating their bifurcations correctly. However, for the ground states of larger systems the deformations are usually not very large – as can be recognized, e.g., from the decreasing amplitudes of δ seen in Fig. 8. It is therefore possible to treat the deformed part of the potential in perturbation theory, using the trace formula (3.16) discussed above. For a slightly quadrupole-deformed billiard the modulation factor (3.15) can be calculated analytically [72, 86]; hereby

the unperturbed system is the spherical billiard. In Fig. 9 we show by contour plots the shell-correction energy δE as a function of particle number N and quadrupole deformation ε_2. The agreement of the quantum-mechanical (left) and semiclassical results (right) demonstrates the quantitative predictive power of the semiclassical theory.

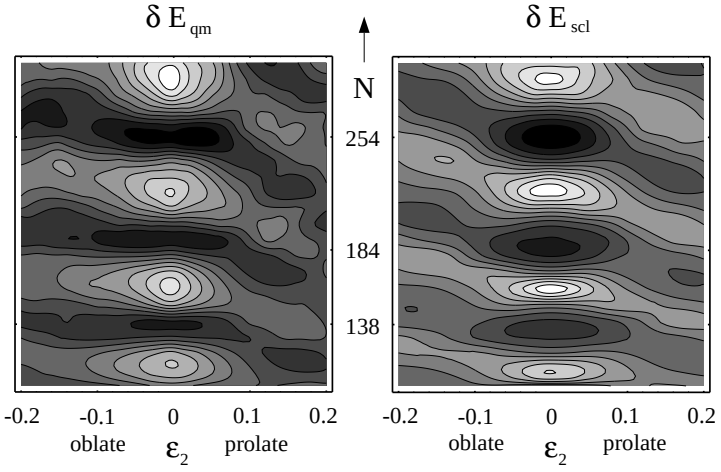

Fig. 9. Contour plots of the shell-correction energy δE for an axially quadrupole-deformed cavity versus particle number N and quadrupole deformation ε_2. *Left:* quantum-mechanical result, *right:* semiclassical result using the perturbative trace formula (3.16); the unperturbed system is the spherical billiard [49]. (From [86].)

3.6 Applications to two-dimensional electronic systems

The recent developments in the fabrication of semiconductor devices on micro- and nanometer scales have opened up interesting new studies of the interplay of classical and quantum mechanics. Quantum dots and other nanostructures with any wanted geometry can be produced at scales where on one hand the coherence length of the electrons is larger than their confinement size, so that quantum interference takes place, but on the other hand their Fermi wave length is small enough so that high quantum numbers are involved and the classical limit is within reach. In addition, these structures are of the order of, or bigger than, the magnetic length scales that can be reached experimentally. Hence, the strength of an applied external magnetic field represents a new degree of freedom for the observation of interesting quantum effects, such as the quantum Hall effect (QHE) and its various manifestations in connection with a laterally confined two-dimensional electron gas (2DEG).

In the following we shall give three applications of the POT to such mesoscopic systems, where the magnetic field plays an important role. In the first one, a circular quantum dot, the observed conductance oscillations could be directly related to the density of states of the confined electrons and hence be interpreted in terms of the trace formula (3.10). The other two examples concern open systems where the conductance is described within the Kubo formalism. The semiclassical description of such systems has been developed in Refs. [87, 88]. In the quantum-mechanical Kubo formula based on the linear response theory, the Green function is replaced by its semiclassical approximation (3.4). The oscillating parts of the longitudinal and transverse conductivity $\delta\sigma_{xx}$ and $\delta\sigma_{xy}$, respectively, with respect to an applied external voltage in the x direction ($z = 0$ is the plane of the 2DEG) can then be expressed in terms of periodic orbits through the following "semiclassical Kubo formulae" (including a spin degeneracy factor 2):

$$\begin{aligned}
\delta\sigma_{xx} &= \frac{4e^2}{h}\frac{1}{A}\sum_{\rm po}\mathcal{C}_{xx}\frac{R_{\rm po}(\tau_\beta)\,F_{\rm po}(\tau_s)}{|\det\left(\widetilde{\mathbf{M}}_{po}-\mathbf{1}\right)|^{1/2}}\cos\left(\frac{S_{po}}{\hbar}-\sigma_{po}\frac{\pi}{2}\right), \qquad (3.35)\\
\delta\sigma_{xy} &= \frac{4e^2}{h}\frac{1}{A}\sum_{\rm po}\left(\frac{1}{e}\frac{\partial S_{po}}{\partial B}+\mathcal{C}_{xy}\right)\frac{R_{\rm po}(\tau_\beta)\,F_{\rm po}(\tau_s)}{|\det\left(\widetilde{\mathbf{M}}_{po}-\mathbf{1}\right)|^{1/2}}\cos\left(\frac{S_{po}}{\hbar}-\sigma_{po}\frac{\pi}{2}\right).
\end{aligned}$$

Here S_{po}, σ_{po}, and $\widetilde{\mathbf{M}}_{po}$ have the same meaning as in the trace formulae presented in Sect. 3.2 above; all are evaluated at the Fermi energy E_F. A finite temperature T is included in the factor $R_{\rm po}(\tau_\beta) = (T_{po}/\tau_\beta)/\sinh(T_{po}/\tau_\beta)$ with the period $T_{po} = \partial S_{po}/\partial E$ and $\tau_\beta = \hbar/(\pi kT)$. Damping due to a finite mean-free path is included by the factor $F_{\rm po}(\tau_s) = \exp\left[-T_{po}/(2\tau_s)\right]$, where $\tau_s = m^*\mu/e$ is the scattering time extracted from the experimental mobility μ, and m^* is the effective mass of the electrons. A is the effective area of the investigated device, and $\mathcal{C}_{ij}$ are the velocity-velocity correlation functions of the periodic orbit, defined by

$$\mathcal{C}_{ij} = \int_0^\infty dt\, e^{-t/\tau_s}\int_0^{T_{po}} d\tau\, v_i(\tau)\, v_j(t+\tau) \qquad (i,j=x,y) \qquad (3.36)$$

in terms of the velocities $v_i(t) = p_i(t)/m^*$ of the periodic orbits.

3.6.1 Conductance oscillations in a circular quantum dot

In a circular quantum dot with approximately 1200 - 1500 confined electrons, the conductance was measured [89, 90] as a function of an applied external (perpendicular) magnetic field B and of the applied gate voltage V_{g1} that defined the effective radius of the confined 2DEG. Regular oscillations of the conductance as a function of both V_{g1} and weak field strength B in the milli-Tesla domain were observed, as shown in the left-hand part

of Fig. 10. A semiclassical reproduction of these oscillations in terms of the trace formula of a circular billiard was given in Ref. [91] and is shown in the right-hand part of Fig. 10. Both the experiment and the semiclassical analysis are well described in the quoted literature; we just summarize the essential conclusions here.

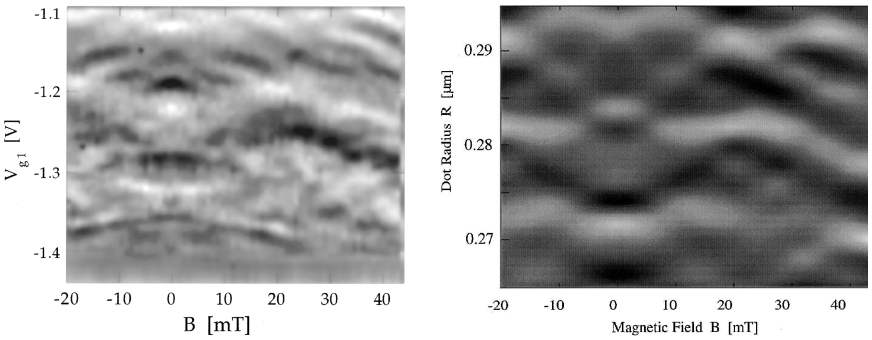

Fig. 10. Gray-scale plots of conductance of a circular quantum dot, plotted versus gate voltage (vertical axis) and magnetic field (horizontal axis). *Left:* experimental result, *right:* semiclassical result using the circular billiard model including the magnetic field in first-order perturbation. (From [91].)

Like in the large metal clusters, the selfconsistent mean field of this quantum dot is expected to have steep walls due to the strong mutual Coulomb repulsion of the trapped electrons. Hence, a two-dimensional circular billiard is a good first-order model. The period of the oscillation in the vertical direction, i.e., as a function of the dot radius R, is given exactly like for the spherical metal clusters by the average length of the leading periodic orbits. In contrast to the three-dimensional spherical billiard, all orbits in a two-dimensional circular billiard have the same one-dimensional degeneracy, and the leading orbit here is the diameter orbit. Using the average length of the diameter and the triangular orbits leads, indeed, to the correct period of the vertical oscillations seen in Fig. 10. (Note, however, that the number of electrons and the radii R were only known approximately here.) The oscillation as a function of a weak magnetic field B is well understood in perturbation theory where only the first-order corrections to the actions S_{po} are taken into account. The modulation factor (3.15) then becomes [91]

$$\mathcal{M}_{po} = \cos\left(\frac{e}{\hbar c} F_{po} B\right) , \tag{3.37}$$

where F_{po} is the *area* included by the orbit *po*. The origin of this modulation factor is just the Aharonov-Bohm (AB) phase of a charged particle surrounding a magnetic field, i.e., the magnetic flux included by the electron's orbit. Here the phase adds to the classical action, the sign of the

flux depending on the orientation of the orbit with respect to the B field. The summation over both directions yields the cosine factor in (3.37). The period of these oscillations for weak B – often called "AB oscillations" – are here essentially given by the shortest orbit with a non-zero area, i.e., by the triangular orbit. This example shows how through the introduction of a weak magnetic field, one is able to "measure" not only the average length, but independently also the average area of the leading periodic orbit(s).

Similar AB oscillations have also been observed in a quantum dot with an equilateral triangular shape [92,93]. In the steep-wall limit, one may use a triangular billiard whose exact trace formula is known analytically [4]; the period of the measured AB oscillations could, indeed, be understood by the area of the shortest periodic orbit of this system. A challenging speculation was proposed for the study of a triangular quantum dot with open contacts and a small number of electrons [92,94]. Neglecting the Coulomb repulsion, the potential of the electrons then is given to lowest order by the famous Hénon-Heiles potential [95] which has mixed classical dynamics. The semiclassical description of its level density using the Gutzwiller theory has been very successful (see Ref. [70] and earlier papers quoted therein). It would be interesting to observe the transition from regular to chaotic motion by tuning the Fermi energy of the electrons. This has, however, not been realized experimentally so far.

Before turning to open nanostructures, we conclude this section on quantum dots by mentioning that for the disk billiard in arbitrarily strong homogeneous magnetic fields, an analytical trace formula has been developed in Ref. [96]. Magnetic properties of quantum dots and dot arrays have also been investigated within the POT [97,98].

3.6.2 Integer quantum Hall effect in the two-dimensional electron gas

An unexpected semiclassical interpretation of the integer QHE was recently proposed by Blaschke [99]. In a typical Hall bar experiment, one measures the transverse (Hall) resistivity ρ_{xy} and the longitudinal resistivity ρ_{xx} with respect to an applied electric voltage in the x direction; the 2DEG is confined to the $z = 0$ plane. The elements of the resistivity tensor ρ_{ij} are given by inverting the conductivity tensor σ_{ij}, and their oscillating parts can thus be calculated semiclassically from the Kubo trace formulae (3.35). The periodic orbits of a 2DEG in a transverse magnetic field are simply the cyclotron orbits whose properties are easily calculated; their continuous degeneracy cancels the factor A. Adding the average resistivities, which are given within the classical Drude model, yields the results shown in Fig. 11. The solid lines give the results obtained by keeping only the lowest-order terms in $\hbar$ of the trace formula (3.35). They correspond to the classical Hall resistivity ρ_{xy} which is linear in B, and to the longitudinal resistivity ρ_{xx} exhibiting the typical Shubnikov-de Haas oscillations. (These are easily

understood semiclassically in terms of the magnetic flux surrounded by the cyclotron orbits which is proportional to $1/B$; see, e.g., Ref. [4].) To lowest order in $\hbar$, the POT is not able to reproduce the plateaux in the Hall resistivity. However, when adding the (only! – see Ref. [99]) $\hbar$ correction coming into the term proportional to $\partial S_{po}/\partial B$ in the trace formula (3.35) for $\delta\sigma_{xy}$ (dashed lines), one obtains the plateaux in ρ_{xy} characteristic of the integer QHE; the influence of this correction on ρ_{xx} is very small.

When the 2DEG is modulated laterally by an "antidot superlattice", interesting commensurability peaks can be observed in the longitudinal resistivity, which correspond to electrons trapped on specific cyclotron orbits that fit around one or more antidots [100]. At low temperatures, small AB oscillations in ρ_{xx} become observable and can be qualitatively reproduced [101] by the interference of the most important periodic orbits via the trace formulae Eq. (3.35). (See Ref. [101] for a mini-review of the so-called "Weiss oscillations".)

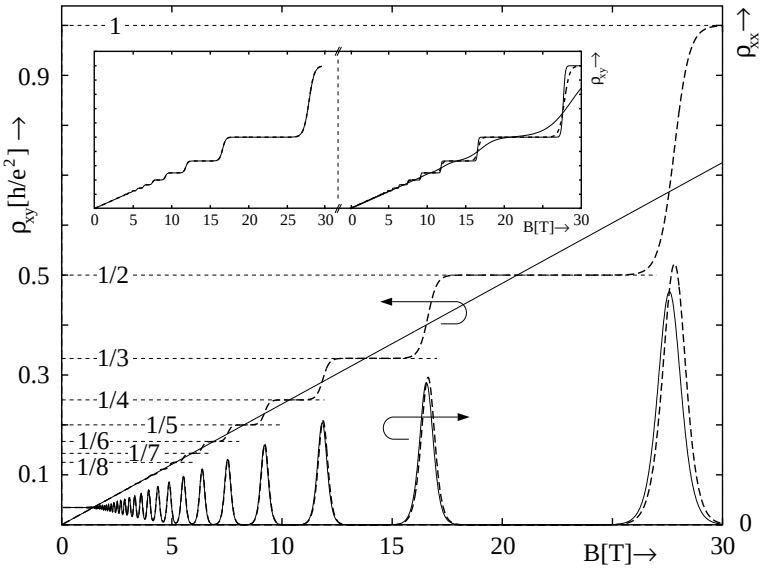

Fig. 11. Semiclassical calculation of the transverse Hall resistivity ρ_{xy} (left axis) and the longitudinal resistivity ρ_{xx} (right axis) of the 2DEG in a transverse magnetic field B. ρ_{xx} shows the typical $1/B$-periodic Shubnikov-de Haas oscillations. ρ_{xy} exhibits the plateaux corresponding to the integer QHE. Solid lines are obtained including only the lowest-order terms in the semiclassical Kubo formula (3.35). Dashed lines include the only $\hbar$-correction to the first term of $\delta\sigma_{xy}$ in (3.35). The inserts illustrate small variations of the mobility of the electrons (left) and of the temperature (right). (From [99].)

3.6.3 Conductance oscillations in a channel with antidots

Our last example is a mesoscopic arrangement in which the electrons of a 2DEG are confined laterally to a channel of width $\sim 1.0\,\mu$m. Two antidots represent obstacles to the electric current through the channel; the effective radius of these antidots can be regulated by an applied gate voltage V_g. Fig. 12 shows an SEM photograph of the experimental gate structure [102]. The longitudinal conductance G_{xx} along the channel has been measured for various strengths of a perpendicular magnetic field B and gate voltages V_g [102,103]. Like in the case of antidot supperlatices [100], a commensurability minimum in the average conductance has been observed near those values of B for which a cyclotron orbit fits around the antidots.

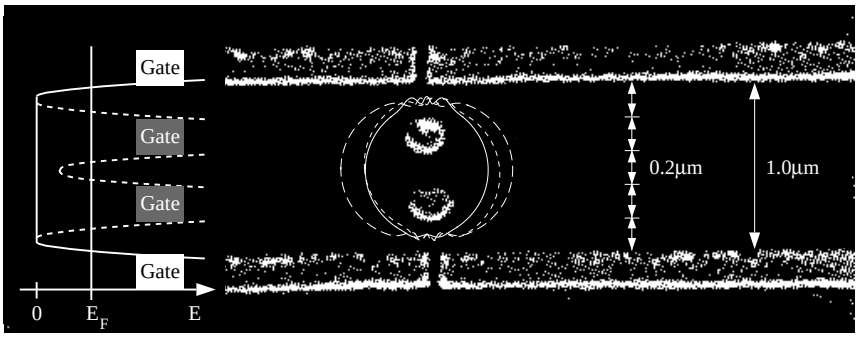

Fig. 12. SEM photograph of the gate structure of a mesoscopic channel with two antidots [102] (without contacts). *Left:* Model potential used for the calculations. *Center:* Typical periodic orbits encircling the antidots. (From [104].)

Small observed AB oscillations around the average part of G_{xx} can again be interpreted semiclassically [99, 104] as interferences between the leading periodic orbits (a few of them are shown in Fig. 12 by solid and dashed white lines) through the trace formulae (3.35). The result of the semiclassical calculation of δG_{xx} is shown in Fig. 13; hereby the parameters of the model potential used to describe the lateral confinement (including the antidots) have been optimized [99]. Like in the case of the Weiss oscillations [101], the amplitude had to be adjusted since the semiclassical Kubo formula is not able to reproduce quantitatively the amplitude of the oscillations.

An interesting phenomenon is observed when varying both the magnetic field B and the gate voltage V_g, and plotting the loci of the oscillation maxima in δG_{xx}. These arrange themselves, as seen in Fig. 14 (a), along smooth lines whose slopes are well understood in terms of the B and V_g dependence of the actions S_{po} of the leading periodic orbits. However, some characteristic dislocations occur at apparently random places in the (B, V_g)

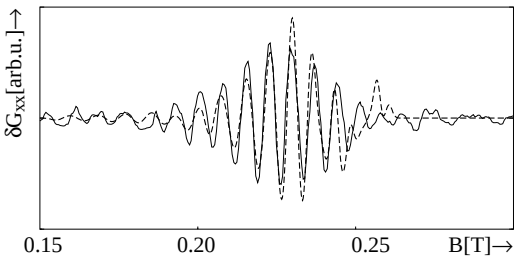

Fig. 13. Oscillating part of the conductance δG_{xx} (in arbitrary units) versus magnetic field strength B (in Tesla). *Solid line:* experiment for $V_g = -1.50$ Volts [103]; *dashed line:* semiclassical result with optimized potential parameters [99].

plane, as emphasized by the boxes. In the semiclassical analysis, they originate from successive bifurcations of periodic orbits: the different orbit generations lead to different slopes in Fig. 14 (b), and these do not match near the loci in the (B, V_g) plane (shown for some leading orbits by gray-shaded thick lines) along which the bifurcations occur. Although the theory does not fit the experiment globally (at least 10 different orbit families contribute), the local agreement near the dislocations is excellent; see the box in Fig. 14 (c). Thus, orbit bifurcations *can* be "seen" in the experiment!

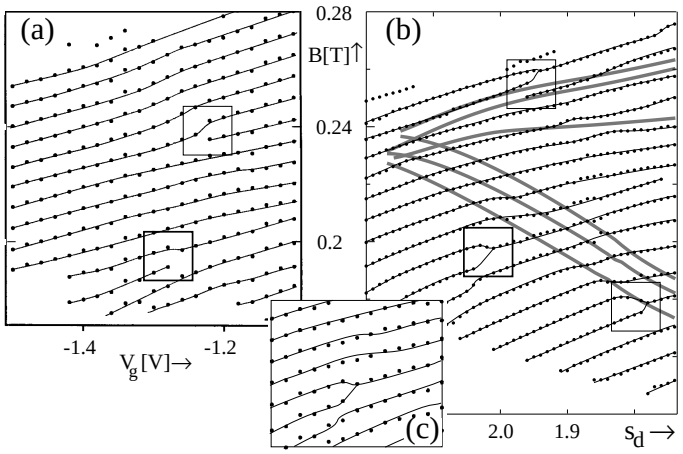

Fig. 14. Maximum positions of δG_{xx} versus B (vertical axes) and V_g (horizontal axes). (a) Experimental values [103]. (b) Semiclassical results [104]; s_d is the antidot radius regulated by V_g; approximately we have $s_d \propto V_g$; the gray-shaded lines correspond to the loci of bifurcations of some leading orbit families. (c) Behaviour near a dislocation (dots: experiment; lines: semiclassical results). (From [104].)

4 Local-current approximation for linear response

We shall in this final section present a semiclassical approach to the collective excitation spectrum of a finite interacting fermion system. The semiclassical aspect here pertains to the calculation of the excitation energies, starting from a ground state that has been obtained either quantum-mechanically or semiclassically in the mean-field approximation. This approach is based on the use of generalized sum rules [105] and is particularly well suited for the description of collective excitations such as giant resonances in nuclei (see Ref. [106] for a review) or plasmon resonances in metal clusters (see Sect. IV.C of the review article [31] on metal clusters). For the latter application, this approach has been developed first within the ETF framework [27] and later in connection with the Kohn-Sham formalism, where it was shown [107] to be an approximation to the random phase approximation (RPA). Since it makes use of localized collective current distributions, it was termed "local RPA" (LRPA, see also Refs. [108, 109]). The method can, however, be derived [110] from the most general quantum-mechanical equations of motion that yield the exact excitation spectrum; the basic semiclassical assumption is, as previously, that the collective currents are given by local functions of $\mathbf{r}$. We therefore propose [111] to term this approach the "local-current approximation" (LCA) which does not restrict its name to further approximations inherent in the RPA.

We first state in Sect. 4.1 the quantum-mechanical equations of motion and relate them to a variational principle, and in Sect. 4.2 we sketch briefly the variational equations that are obtained if the basic excitation operators are assumed to be local functions of $\mathbf{r}$. In Sect. 4.3 we give a practical way to solve these equations approximately in finite basis sets and give a physical interpretation of the LCA, and in the remaining parts we shall present some results of applications to metal clusters.

4.1 Quantum-mechanical equations of motion

In this and the next subsection we follow closely Ref. [110]. We consider a many-particle system defined by the Hamiltonian $H = T + V$, where V includes external one-body potentials and the two-body interaction. (For simplicity, we omit in the following the "hat" symbol "$\hat{}$" to indicate operators.) The exact ground state $|0\rangle$ and excited states $|\nu\rangle$ are given by the stationary Schrödinger equation

$$H|\nu\rangle = E_\nu|\nu\rangle = (E_0 + \hbar\omega_\nu)|\nu\rangle\,. \qquad \nu = 0, 1, 2, \ldots \tag{4.1}$$

It is a matter of standard many-body theory (see, e.g., Refs. [112–114]) to rewrite (4.1) in the form of the following equations of motion

$$\langle 0|\mathcal{O}_\nu[H, \mathcal{O}_\nu^\dagger]|0\rangle \;=\; \hbar\omega_\nu\langle 0|\mathcal{O}_\nu\mathcal{O}_\nu^\dagger|0\rangle\,, \tag{4.2}$$

$$\langle 0|\mathcal{O}_\nu[H,\mathcal{O}_\nu]|0\rangle \quad = \quad \hbar\omega_\nu\langle 0|\mathcal{O}_\nu\mathcal{O}_\nu|0\rangle = 0\,, \tag{4.3}$$

where the operators $\mathcal{O}_\nu$ and $\mathcal{O}_\nu^\dagger$ are defined as the creation and annihilation operators of the excited states:

$$\mathcal{O}_\nu^\dagger|0\rangle = |\nu\rangle, \qquad \mathcal{O}_\nu|\nu\rangle = |0\rangle, \qquad \text{and} \qquad \mathcal{O}_\nu|0\rangle = 0\,. \tag{4.4}$$

The exact solutions of the equations (4.2,4.3) are unknown for most systems, as are those of the Schrödinger equation (4.1). Several approximative ways to find the excited energies $\hbar\omega_\nu$ and/or their eigenstates have been developed; they differ in the approximations used for the ground state $|0\rangle$ and the explicit form of the excitation operators $\mathcal{O}_\nu^\dagger$. In the Tam-Dancoff scheme one starts from the HF approximation, where the ground state $|0\rangle = |\mathrm{HF}\rangle$ is a Slater determinant, and the excitation operators are taken to be simple one-particle-one-hole ($1p$-$1h$) operators. In the small-amplitude limit of the time-dependent HF theory, the so-called random phase approximation (RPA) is obtained by admitting $2p$-$2h$ excitations in the ground state

$$|0\rangle = |\mathrm{RPA}\rangle = \left(1 + \sum_{pp'hh'} \gamma^{pp'hh'} a_p^\dagger a_{p'}^\dagger a_h a_{h'}\right)|\mathrm{HF}\rangle\,, \tag{4.5}$$

and taking the excitation operators to be linear combinations of $1p$-$1h$ excitations of the form:

$$\mathcal{O}_\nu^{\dagger\,(RPA)} = \sum_{ph}\left(x_\nu{}^{ph} a_p^\dagger a_h - y_\nu{}^{ph} a_h^\dagger a_p\right). \tag{4.6}$$

In the above definitions, $a^\dagger$ and a are the single-particle creation and annihilation operators for particle states (with $\varepsilon_p, \varepsilon_{p'} > E_F$) and hole states (with $\varepsilon_h, \varepsilon_{h'} \le E_F$), respectively, with respect to the HF ground state. We refer again to the literature for the details of these approximations [114].

For the following it is now essential that a variational principle can be formulated [110] which is exactly equivalent to solving the general equations of motion (4.2,4.3). For that we introduce a Hermitian operator Q that can be interpreted as a generalized coordinate. To find the lowest excited state, one has to solve the variational equation

$$\frac{\delta E_3[Q]}{\delta Q} = 0\,, \tag{4.7}$$

where $E_3[Q]$ is defined by

$$E_3[Q] = \sqrt{\frac{m_3[Q]}{m_1[Q]}}\,, \tag{4.8}$$

and the "moments" m_1 and m_3 (see the discussion of their physical significance in Sect. 4.3 below) are defined as expectation values of multiple commutators

$$m_1[Q] = \frac{1}{2}\langle 0|\,[Q,[H,Q]]\,|0\rangle\,, \tag{4.9}$$

$$m_3[Q] = \frac{1}{2}\langle 0|\,[[H,Q]\,,[[H,Q]\,,H]]\,|0\rangle\,. \tag{4.10}$$

The minimum value of E_3 after variation gives the first excitation energy $\hbar\omega_1$. The corresponding operator Q_1 is written as the linear combination

$$Q_1 \propto \mathcal{O}_1^\dagger + \mathcal{O}_1 \tag{4.11}$$

of the creation and annihilation operators for the first excited state. The second excitation with energy $\hbar\omega_2$ can then be obtained from variation of Q in an operator space that has been orthogonalized to Q_1, and so on. In this way the whole excitation spectrum $\hbar\omega_\nu$ can be successively constructed (see Ref. [110] for the details).

In principle, the *exact* excited states and excitation energies of the system are given by the solutions of the variational equation (4.7). For practical calculations, however, one is forced to make some ansatz for the generally non-local operator Q. If it is taken from the space of particle-hole operators of the form (4.6), then Eq. (4.7) leads precisely to the RPA equations [107]. [Note that the RPA, in a consistent use within the DFT, includes the exchange-correlations effects. In the condensed matter literature, however, the corresponding approach is more often referred to as the "time-dependent LDA" or TDLDA approach, whereas the name RPA is reserved to an approximation which ignores the exchange-correlations effects. Nuclear physicists usually include the exact exchange in their RPA treatment, starting from the HF ground state as implied in Eq. (4.5) above.] Even in this approximation, the equations of motion are very difficult to solve for clusters without any spatial symmetry, e.g., including the ionic structure. In the following we shall discuss a semiclassical approach which makes use of a local approximation to the operator Q and has been successfully used for collective excitations both in nuclear [106] and cluster physics.

4.2 Variational equation for the local current density

Starting from the exact equations of motion defined by the variational principle Eqs. (4.7) – (4.10), we now make the following two approximations. First, we write the ground-state energy as usual in DFT as a functional of the local density, $E = E[\rho(\mathbf{r})]$ as in (2.19), using a standard approximation for the exchange-correlation functional (e.g., the LDA). Second, we assume Q to be a *local function of* $\mathbf{r}$:

$$Q = Q(\mathbf{r})\,. \tag{4.12}$$

Then, for an electronic system where the external potentials are local and the two-body interaction is just the bare Coulomb interaction, the commutator $[H,Q]$ is only given by its kinetic part (i.e., the potential part in H commutes with Q):

$$[H,Q] = [T,Q] = \frac{1}{2}(\nabla\cdot\mathbf{u}) + \mathbf{u}\cdot\nabla\,, \tag{4.13}$$

where

$$\mathbf{u}(\mathbf{r}) = -\frac{\hbar^2}{m}\,\nabla Q(\mathbf{r}) \tag{4.14}$$

is a local velocity field, as will be discussed in Sect. 4.3 below. (Note that only the gradient of the velocity potential $Q(\mathbf{r})$ enters the following development.) The moments (4.9,4.10) are then functionals of the local density $\rho(\mathbf{r})$ and the velocity field $\mathbf{u}(\mathbf{r})$. The moment m_1 is easily found to be

$$m_1[Q] = m_1[\mathbf{u}] = \frac{m}{2\hbar^2}\int \mathbf{u}(\mathbf{r})\cdot\mathbf{u}(\mathbf{r})\,\rho(\mathbf{r})\,d^3r\,. \tag{4.15}$$

The moment $m_3[\mathbf{u}]$ becomes more complicated but can be readily calculated from $\rho(\mathbf{r})$, $\mathbf{u}(\mathbf{r})$, their derivatives, and from the KS wavefunctions, using the current-density functional theory [115]. (See Ref. [110] for the most general expressions for $m_3[\mathbf{u}]$; special cases within the ETF model have been given in Ref. [27].) Performing the variation (4.7) then leads to the following eigenvalue equations for the excitation energy $\hbar\omega$:

$$\frac{\delta m_3[\mathbf{u}]}{\delta u_j(\mathbf{r})} = (\hbar\omega)^2\,\frac{m}{\hbar^2}\,\rho(\mathbf{r})\,u_j(\mathbf{r}) = m\omega^2\,\rho(\mathbf{r})\,u_j(\mathbf{r}) \qquad (j=x,y,z) \tag{4.16}$$

(see Ref. [110] for the explicit form of the left-hand side above). The solution of these equations yields the lowest excitation energy $\hbar\omega = \hbar\omega_1$ and the corresponding velocity field $\mathbf{u}_1(\mathbf{r})$. As sketched above, the second excitation energy $\hbar\omega_2$ is then found by restricting the solution $\mathbf{u}(\mathbf{r})$ of (4.16) to be orthogonal to $\mathbf{u}_1(\mathbf{r})$, and so on.

Due to the complexity of $m_3[\mathbf{u}]$, Eqs. (4.16) represent a set of coupled nonlinear fourth-order partial differential equations for the three spatial components of $\mathbf{u}(\mathbf{r})$, which are close in spirit to the variational equations [116] derived from the so-called fluid dynamical approach [117, 118] developed in nuclear physics. Different from the approximations used there, however, Eqs. (4.16) can be solved using the exact quantum-mechanical KS wavefunctions of the ground state. The semiclassical approximation implied by (4.12) then affects only the collective excitation mechanism.

Eqs. (4.16) are still quite formidable to solve numerically without further restrictions on the form of the velocity fields $\mathbf{u}(\mathbf{r})$. (For some first attempts, see Ref. [110].) An appreciable simplification arises when $\mathbf{u}(\mathbf{r})$ or, equivalently, the operator $Q(\mathbf{r})$, is expanded on a finite basis of local functions, as discussed in the following section.

4.3 Secular equation using a finite basis

We now expand the local excitation operator $Q(\mathbf{r})$ in a finite set of basis functions $Q_n(\mathbf{r})$:

$$Q(\mathbf{r}) \in \{Q_n(\mathbf{r})\}\,. \qquad n = 1, 2, ..., M \tag{4.17}$$

The variational equation (4.7) then becomes simply a secular equation for coupled harmonic vibrations generated by these operators:

$$\det|\mathcal{K}_{mn} - \omega_\nu^2\,\mathcal{B}_{mn}| = 0\,, \qquad m, n = 1, 2, ..., M \tag{4.18}$$

yielding the collective excitation energies $\hbar\omega_\nu$ that represent the finite-basis LCA to the exact spectrum. Here the mass tensor $\mathcal{B}_{mn}$ and the restoring force tensor $\mathcal{K}_{mn}$ are given by

$$\mathcal{B}_{mn} = \hbar^2\langle 0|\,[Q_m, [H, Q_n]]\,|0\rangle\,, \tag{4.19}$$

$$\mathcal{K}_{mn} = \langle 0|\,[[H, Q_m], [[H, Q_n], H]]\,|0\rangle\,, \tag{4.20}$$

which, apart from some reshuffling of constants, are the nondiagonal generalizations of the moments m_1 and m_3 defined in Eqs. (4.9,4.10). After solving Eq. (4.18) one finds the intrinsic local excitation operators $Q_\nu(\mathbf{r})$, which create the states $|\nu\rangle$, as linear combinations of the basis operators $Q_n(\mathbf{r})$:

$$Q_\nu(\mathbf{r}) = \sum_{n=1}^{M} c_n^\nu\, Q_n(\mathbf{r})\,. \tag{4.21}$$

The physical meaning (see also Refs. [27,106,107]) of the operators $Q_\nu(\mathbf{r})$ shall in the following be illustrated in the so-called "scaling approach" [105, 106]. This is the simple case where a collective excitation is created by one single operator $Q(\mathbf{r})$, i.e., using $M = 1$ in (4.17) and (4.18). The collective flow of the particles can be described by a velocity field $\mathbf{v}_\alpha(\mathbf{r}, t)$ which is proportional to $\mathbf{u}(\mathbf{r})$

$$\mathbf{v}_\alpha(\mathbf{r}, t) = \dot{\alpha}(t)\,\mathbf{u}(\mathbf{r})\,, \tag{4.22}$$

so that $Q(\mathbf{r})$ (apart from a constant factor) plays the role of a velocity potential. The collective coordinate $\alpha(t)$, which undergoes harmonic oscillations

$$\alpha(t) = \alpha_0 \sin(\omega t)\,, \tag{4.23}$$

defines the time dependence of the single-particle wavefunctions by

$$\varphi_i(\mathbf{r}, t) = \varphi_i(\mathbf{r}, \alpha(t)) = e^{-\alpha(t)S}\varphi_i(\mathbf{r})\,, \tag{4.24}$$

where the "scaling operator" S is defined by

$$S = [T, Q] = \frac{1}{2}(\nabla \cdot \mathbf{u}) + \mathbf{u} \cdot \nabla. \tag{4.25}$$

Taking the time derivative of (4.24), the time dependent density

$$\rho_\alpha(\mathbf{r},t) = \rho(\mathbf{r},\alpha(t)) = \sum_{\varepsilon_i \le E_F} |\varphi_i(\mathbf{r},\alpha(t))|^2 \tag{4.26}$$

is immediately seen to fulfill the continuity equation

$$\frac{\partial}{\partial t}\rho_\alpha(\mathbf{r},t) + \nabla\cdot\mathbf{j}_\alpha(\mathbf{r},t) = 0\,, \tag{4.27}$$

where

$$\mathbf{j}_\alpha(\mathbf{r},t) = \rho_\alpha(\mathbf{r},t)\,\mathbf{v}_\alpha(\mathbf{r},t) \tag{4.28}$$

is the *local current distribution* describing the collective flow of the excited system. This is the reason why we call the present scheme the "local-current approximation" (LCA) – in contrast to the RPA scheme where the currents are implicitly given by nonlocal particle-hole operators. The mass parameter $\mathcal{B}$ is now given by [cf. (4.15)]

$$\mathcal{B} = m\int \mathbf{u}(\mathbf{r})\cdot\mathbf{u}(\mathbf{r})\;\rho(\mathbf{r})\,d^3r\,, \tag{4.29}$$

and the restoring force parameter $\mathcal{K}$ is obtained from the "scaled" ground-state energy $\langle\alpha|H|\alpha\rangle = E[\rho(\mathbf{r},\alpha)]$ according to

$$\begin{aligned}\mathcal{K} &= \langle 0|\,[S,[S,H]]\,|0\rangle &&= \left[\frac{d^2}{d\alpha^2}\langle 0|\,e^{\alpha S}He^{-\alpha S}\,|0\rangle\right]_{\alpha=0}\\ &= \left[\frac{d^2}{d\alpha^2}\langle\alpha|H|\alpha\rangle\right]_{\alpha=0} &&= \left[\frac{d^2}{d\alpha^2}E[\rho(\mathbf{r},\alpha)]\right]_{\alpha=0}\,.\end{aligned} \tag{4.30}$$

Since $E[\rho(\mathbf{r},\alpha)]$ on the right-hand side can be considered as the potential energy $V(\alpha)$ of a collective Hamiltonian

$$H_{coll}(\alpha,\dot\alpha) = \frac{1}{2}\mathcal{B}\dot\alpha^2 + V(\alpha)\,, \tag{4.31}$$

we see that the solution of Eq. (4.18) in this one-mode picture is just the first excitation energy of (4.31) in the harmonic approximation: $\hbar\omega = E_3(Q) = \sqrt{\mathcal{K}/\mathcal{B}}$. If one identifies the intrinsic excitation operator $Q(\mathbf{r})$ with the external operator Q_{ext} by which the system is probed, this corresponds exactly to the simple sum rule picture [105] (or, in solid state physics, the so-called plasmon pole approximation).

The extension to the LCA scheme with several basis operators (4.17) is now evident: one couples several harmonic oscillators, each corresponding to one individual collective degree of freedom $\alpha_n(t)$, described by a velocity

potential $Q_n(\mathbf{r})$, and diagonalizes this system via Eq. (4.18). This corresponds to a collective Hamiltonian with M coupled degrees of freedom, which in the harmonic approximation becomes

$$H_{coll} = \frac{1}{2} \sum_{m,n=1}^{M} \left(\mathcal{B}_{mn}\, \dot{\alpha}_m \dot{\alpha}_n + \mathcal{K}_{mn}\, \alpha_m \alpha_n \right). \tag{4.32}$$

We now use this method to calculate the response of the system to an external field, characterized by an operator Q_{ext}. The strength function $S_{Q_{ext}}(E)$ is defined by

$$S_{Q_{ext}}(E) = \sum_{\nu \neq 0} |\langle \nu | Q_{ext} | 0 \rangle|^2 \, \delta(E - \hbar\omega_\nu) \,. \tag{4.33}$$

Hereby the spectrum $\{|\nu\rangle, \hbar\omega_\nu\}$ may be the exact one given by Eqs. (4.2) - (4.4), or that obtained in any approximation. From the strength function one defines the k-th energy-weighted moments $m_k(Q_{ext})$:

$$m_k(Q_{ext}) = \int_0^\infty E^k \, S_{Q_{ext}}(E)\, dE = \sum_{\nu \neq 0} (\hbar\omega_\nu)^k \, |\langle \nu | Q_{ext} | 0 \rangle|^2 \,, \tag{4.34}$$

which can be related to experimental observables. For instance, the photoabsorption cross section $\sigma(\omega)$ is in the long-wavelength limit given by

$$\sigma(\omega) = \frac{4\pi\omega}{3c} \, S_D(E = \hbar\omega) \,, \tag{4.35}$$

where

$$D = Q_{ext} = e\, z \tag{4.36}$$

is the electric dipole operator and ω the frequency of the external electric field (assumed to be polarized in the z-direction). The above moments are then simply given as the following integrals over the cross section:

$$m_1(D) = \int \sigma(\omega)\, d\omega \,, \qquad m_3(D) = \int \omega^2 \sigma(\omega)\, d\omega \,. \tag{4.37}$$

The moment $m_1(D)$ can be calculated immediately and yields the model-independent Thomas-Reiche-Kuhn sum rule (in atomic physics called the "f-sum rule"):

$$m_1(D) = \int \sigma(\omega)\, d\omega = 2\pi^2 \, \frac{e^2}{mc} \, Z \,, \tag{4.38}$$

where Z is the number of electrons taking part in the collective excitation. The experimental verification of the sum rule (4.38) thus helps to identify the collective nature of a resonance. The observed plasmon resonances in

alkali clusters typically account for ~ 60 – 80 % of the total dipole strength (see, e.g., Sect. VIII of Ref. [40]).

The moment $m_{-1}(Q_{ext})$ can be shown [119, 120] to be proportional to the static polarizability α_{pol} of the ground state with respect to the external field Q_{ext}

$$m_{-1}(Q_{ext}) = \frac{1}{2}\,\alpha_{pol}(Q_{ext})\,. \tag{4.39}$$

This gives a convenient way to calculate static polarizabilities once the collective spectrum of a system is known.

By construction, the spectrum $\{|\nu\rangle, \hbar\omega_\nu\}$ obtained by solving the LCA secular equations (4.18) fulfills the sum rules $m_1(Q_{ext})$ and $m_3(Q_{ext})$ exactly, if the operator Q_{ext} is contained in the basis $\{Q_n(\mathbf{r})\}$. [This is, of course, trivial in the one-mode picture discussed above, where the only local operator $Q(\mathbf{r})$ is taken to be the external excitation operator.] It is now a matter of physical intuition to guess the form of the intrinsic excitation operators of a given system by making a suitable choice of the local basis $\{Q_n(\mathbf{r})\}$. In connection with the optic response, it is obvious that the dipole operator D (4.36) should be contained in this basis. Suitable basis sets for applications to metal clusters will be given in the following subsection.

4.4 Applications to metal clusters

For applications of the finite-basis LCA to metal clusters using the jellium model, the following set of local operators in polar coordinates (r, θ, ϕ) has proven to be very efficient and simple to use [27, 107]:

$$Q^p_{lm}(\mathbf{r}) = -e\, r^p\, \frac{1}{2}\left[Y_{lm}\,(\vartheta,\varphi) + Y^*_{lm}\,(\vartheta,\varphi)\right]\,, \tag{4.40}$$

where $Y_{lm}(\theta,\phi)$ are the spherical harmonics in polar coordinates (r,θ,ϕ); $m = 0$ and $m = \pm 1$ correspond to the different polarizations of the external dipole field. For spherical clusters, where the angular momentum l is a conserved quantum number, a set of four to eight basis operators with $l = 1$ and $p = 1, 3, 5, \ldots$ or $p = 1, 4, 7, \ldots$ are often sufficient to get a good estimate of the lowest states of the collective dipole spectrum, in particular in the jellium model. For deformed clusters, several values of l must, of course, be included in the basis (see, e.g., Ref. [121] for calculations in the deformed jellium model). In calculations where the ionic structure is taken into account [122, 123], the following set of operators has been added to the basis set (4.40):

$$Q^k_{lm}(\mathbf{r}) = -e\, j_l(kr)\, \frac{1}{2}\left[Y_{lm}\,(\vartheta,\varphi) + Y^*_{lm}\,(\vartheta,\varphi)\right]\,, \tag{4.41}$$

where $j_l(x)$ are the spherical Bessel functions. We shall in the following present some results obtained with these basis sets.

4.4.1 Optic response in the jellium model

As a first test of the LCA, we show in Fig. 15 the collective spectrum obtained in Ref. [107] for the spherical neutral clusters Na_8 and Na_{20}, calculated in the spherical jellium model by solving the KS equation in LDA. The upper parts give the results of a fully microscopical RPA calculation [124]; the lower parts give the results of the LCA using the basis (4.40). The main peak is split in the RPA result for Na_{20}; this is understood in terms of an interference of the collective oscillation with a specific $1p1h$ excitation [124] (so-called "Landau fragmentation"). It remains to be seen if a solution of the unrestricted LCA variational equations (4.16) is able to reproduce this splitting [111]. Apart from this, the agreement between RPA and LCA is excellent; in particular, the m_3 and m_1 dipole sum rules exhausted by the main peak(s) below 3.2 eV agree within less than one percent.

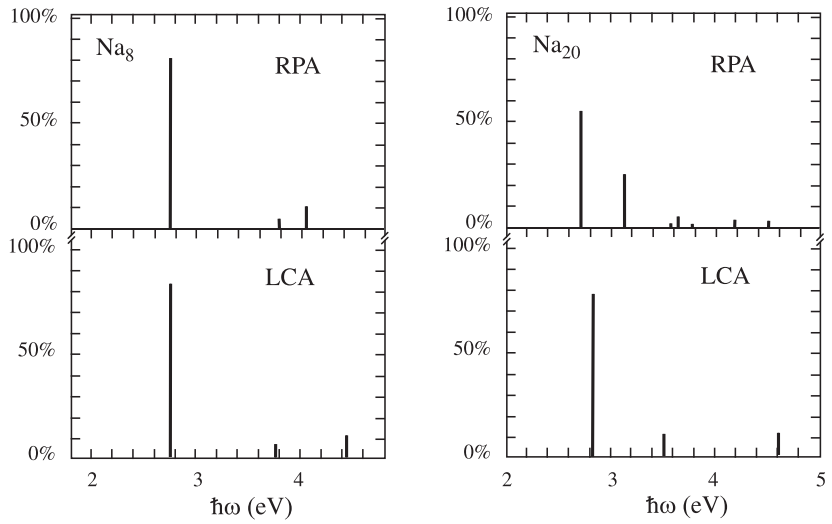

Fig. 15. Collective spectra of the spherical clusters Na_8 and Na_{20} obtained in the jellium model. The positions of the vertical lines give the eigenenergies found by solving the secular equation (4.18), their heights give their percentage of the dipole m_1 sum rule. The ground state was obtained by solving the KS equations. *Upper panels:* RPA spectrum [124], *lower panels:* LCA spectrum [107].

Fig. 16 shows static electric dipole polarizabilities of sodium clusters, plotted versus the cluster radii R_I. Black dots with error bars are the experimental values; the other symbols are results of spherical jellium-model calculations. The square boxes were obtained in the TDLDA [29, 125, 126]. They are perfectly well reproduced by the LCA calculations of Ref. [107]

via the m_{-1} sum rule relation (4.39), using the operator basis (4.40) and the full KS approach for the ground state. When the latter is replaced by a variational ETF calculation, the average results shown by the dashed line are obtained [27].

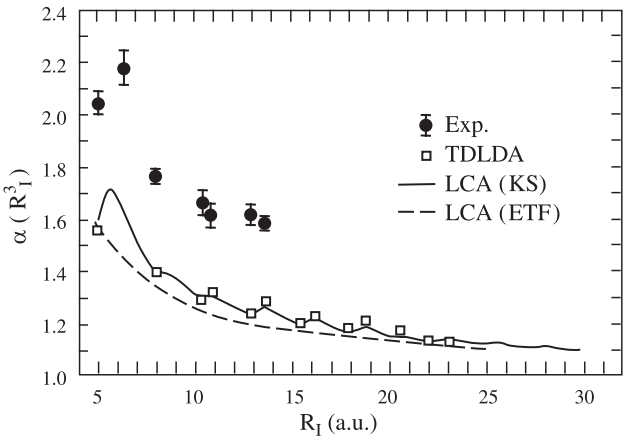

Fig. 16. Static electric dipole polarizabilities α of sodium clusters. *Dots with error bars:* experimental results [80]. *Open squares:* TDLDA results [29,125,126]. *Solid line:* LCA result using the m_{-1} sum rule from the KS ground state [107]. *Dashed line:* LCA result using the m_{-1} sum rule from the ETF ground state [27].

The main discrepancy between theory and experiment is here due to the lack of ionic structure in the jellium model. Inclusion of ionic structure gives a substantial improvement of the theoretical results [127,128], in particular if the finite temperature is also taken into account [129,130].

4.4.2 Optic response with ionic structure

We finally give some examples of LCA calculations that include the ionic structure. In the "cylindrically averaged pseudopotential scheme" (CAPS) [131], the ions are treated three-dimensionally by Monte-Carlo simulated annealing using a local pseudopotential, but only the axially averaged total ionic potential is included into the DFT treatment of the electrons. This has the advantage that the KS equations only have to be solved on a two-dimensional grid (with cylindrical symmetry), which allows to treat larger systems with an affordable numerical effort. Kümmel [110] has constructed a local "soft" pseudopotential that reproduces the correct bulk properties of sodium and at the same time the $3s$ energy level of the valence electron in the sodium atom (see also Refs. [123,132]). It should therefore be suitable

for the use in clusters that interpolate from the atom to the bulk. Indeed, the ground-state structures obtained with this pseudopotential in CAPS calculations reproduce the experimental bond lengths in the smallest sodium clusters as well as all-electron *ab initio* calculations [110, 127].

In Fig. 17 (top part) we show the photoabsorption spectra obtained for Na_2 and Na_8 in CAPS calculations using the LCA for the collective excitation spectrum (note that the widths are phenomenological like in most TDLDA or RPA calculations). The positions of the main peaks reproduce the experimental peaks (bottom part) very well. Also shown (middle part) is the result of a typical TDLDA calculation [133] using the Troullier-Martins pseudopotential, which yields a slight blue shift of the peaks due to a systematic underestimation of the bond lengths.

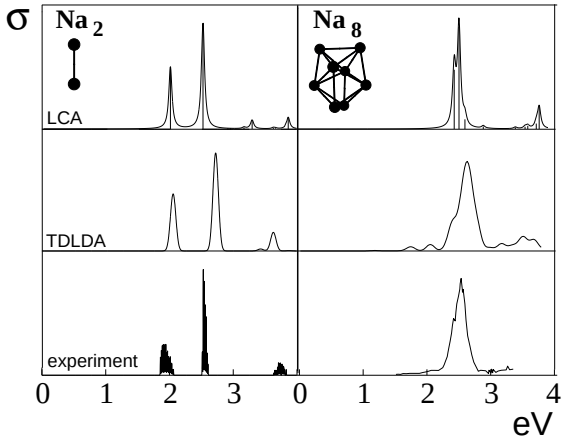

Fig. 17. Photoabsorption cross section σ (in arbitrary units) versus energy (in eV) for the neutral clusters Na_2 (left) and Na_8 (right). *Top panels:* LCA results [110,127]; *center panels:* TDLDA results [133]; *bottom panels:* experimental results [134]. (From [110].)

Fig. 18 shows the structures and collective dipole spectra obtained for the charged clusters Na_{27}^+ and Na_{41}^+ using the same scheme. Again, the LCA calculations [122] yield an excellent reproduction of the experimental peaks in the photoabsorption cross section, including the high-energy shoulder seen in Na_{41}^+.

We conclude by noting that an approximate icosahedral structure was found in the same set of CAPS calculations for the ground state of the Na_{55}^+ cluster [123, 132]; it has been confirmed (with only minor non-axial deviations) in DFT-LDA molecular dynamics calculations without symmetry restrictions [135].

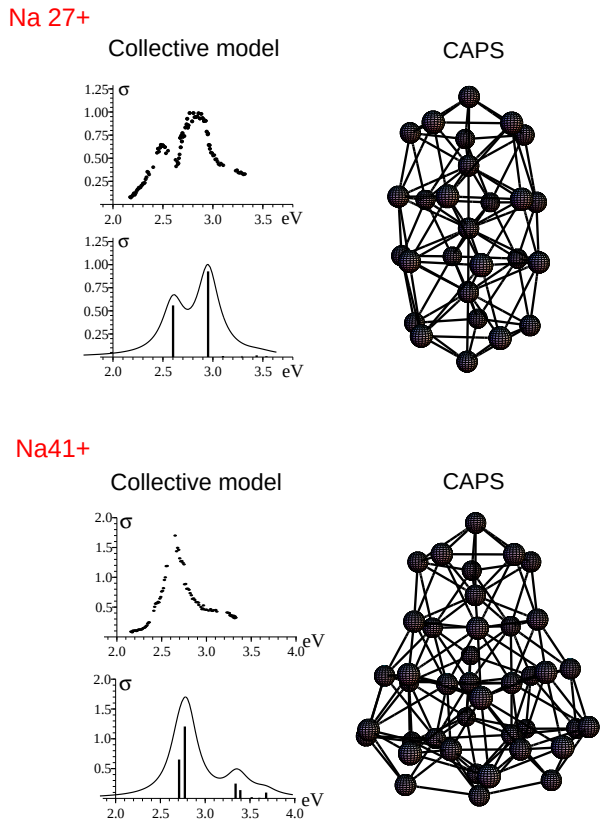

Fig. 18. *Right:* ionic structures of Na_{27}^+ and Na_{41}^+ obtained in the CAPS [122]. *Left:* photoabsorption cross sections σ in arbitrary units, plotted versus energy in eV. *Upper parts, dots:* experimental results [136]; *lower parts:* theoretical results obtained in the LCA [122].

Acknowledgments

I have profited substantially from my collaborators and students. Without their contributions and encouragement much of the material included in these lectures would not exist. I am particularly indebted to Joachim Blaschke and Stephan Kümmel for allowing me to include some partially unpublished results of their Ph. D. work. Several parts of the work presented here were supported by the Deutsche Forschungsgemeinschaft.

References

[1] R. M. Dreizler and E. K. U. Gross: *Density Functional Theory* (Springer, Berlin, 1990).

[2] V. M. Strutinsky, Nucl. Phys. **A 122**, 1 (1968), and earlier references quoted therein.

[3] R. K. Bhaduri and C. K. Ross, Phys. Rev. Lett. **27**, 606 (1971).

[4] M. Brack and R. K. Bhaduri: *Semiclassical Physics*, Frontiers in Physics, Vol. 96 (Addison-Wesley, Reading, USA, 1997).

[5] L. H. Thomas, Proc. Camb. Phil. Soc. **23**, 195 (1926); E. Fermi, Z. Phys. **48**, 73 (1928).

[6] N. H. March: *Self-consistent Fields in Atoms* (Pergamon Press, Oxford, 1975).

[7] E. H. Lieb, Rev. Mod. Phys. **53**, 603 (1981).

[8] E. Wigner, Phys. Rev. **40**, 749 (1932); J. G. Kirkwood, Phys. Rev. **44**, 31 (1933).

[9] M. Abramowitz and I. A. Stegun: *Handbook of Mathematical Functions* (Dover Publications, New York, 9th printing, 1970).

[10] B. Van der Pohl and H. Bremmer: *Operational Calculus* (Cambridge University Press, Cambridge, 1955).

[11] B. Grammaticos and A. Voros, Ann. Phys. (N. Y.) **123**, 359 (1979); **129**, 153 (1980).

[12] C. H. Hodges, Can. J. Phys. **51**, 1428 (1973).

[13] M. Brack, B. K. Jennings, and Y. H. Chu, Phys. Lett. **65 B**, 1 (1976).

[14] C. F. v. Weizsäcker, Z. Phys. **96**, 431 (1935).

[15] R. O. Jones and O. Gunnarsson, Rev. Mod. Phys. **61**, 689 (1989).

[16] F. Perrot, Phys. Rev. **A 20**, 586 (1979).

[17] M. Brack, Phys. Rev. Lett. **53**, 119 (1984); *ibid.* (Erratum) **54**, 851 (1985).

[18] J. Bartel, M. Brack, and M. Durand, Nucl. Phys. **A 445**, 263 (1985).

[19] M. Brack, C. Guet, and H.-B. Håkansson, Phys. Reports **123**, 275 (1985).

[20] D. R. Murphy and W. P. Wang, J. Chem. Phys. **72**, 429 (1980).

[21] C. Guet and M. Brack, Z. Phys. **A 297**, 247 (1980).

[22] M. Centelles, X. Viñas, M. Barranco, and P. Schuck, Ann. Phys. (N. Y.) **221**, 165 (1993).

[23] J. Caro, E. Ruiz Arriola, and L. L. Salcedo, J. Phys. G 22, 981 (1996).

[24] P. Hohenberg and W. Kohn, Phys. Rev. **136**, B864 (1964).

[25] M. Centelles, M. Pi, X. Viñas, F. Garcias, and M. Barranco, Nucl. Phys. **A 510**, 397 (1990).

[26] E. Engel and J. P. Perdew, Phys. Rev. **B 43**, 1331 (1991).

[27] M. Brack, Phys. Rev. **B 39**, 3533 (1989).

[28] M. Seidl and M. Brack, Ann. Phys. (N. Y.) **245**, 275 (1996).

[29] W. Ekardt, Phys. Rev. **B 29**, 1558 (1984).

[30] O. Genzken and M. Brack, Phys. Rev. Lett. **67**, 3286 (1991).

[31] M. Brack, Rev. Mod. Phys. **65**, 677 (1993).

[32] M. Seidl, K.-H. Meiwes-Broer, and M. Brack, J. Chem. Phys. **95**, 1295 (1991).

[33] M. Seidl, J. P. Perdew, M. Brajczewska, and C. Fiolhais, Phys. Rev. **B 55**, 13288 (1997); J. Chem. Phys. **108**, 8182 (1998).

[34] P. Blaise, S. A. Blundell, and C. Guet, Phys. Rev. **B 55**, 15856 (1997).

[35] A. Domps, E. Suraud, and P.-G. Reinhard, Eur. Phys. J. **D 2**, 191 (1998); A. Domps, P.-G. Reinhard, and E. Suraud, Phys. Rev. Lett. **80**, 5520 (1998).

[36] A. Aguado, J. M. López, J. A. Alonso, and M. J. Stott, J. Chem. Phys. **111**, 6026 (1999).

[37] S. A. Blundell, C. Guet, and R. Zope, Phys. Rev. Lett. **84**, 4826 (2000).

[38] W. D. Myers and W. J. Swiatecki, Ann. Phys. (N. Y.) **55**, 395 (1969).

[39] M. Seidl, Ph. D. Thesis (University of Regensburg, 1994, unpublished).

[40] W. A. de Heer, Rev. Mod. Phys. **65**, 611 (1993).

[41] C. Fiolhais and J. P. Perdew, Phys. Rev. **B 45**, 6207 (1992).

[42] M. Seidl and J. P. Perdew, Phys. Rev. **B 50**, 5744 (1994).

[43] N. Bohr, Phil. Mag. (Series 6) **26**, 1, 857 (1913).

[44] A. Pais: *Niels Bohr's Times* (Clarendon Press, Oxford, 1991).

[45] G. Wentzel, Z. Phys. **38** 518 (1926); H. Kramers, Z. Phys. **39**, 828 (1926); L. Brillouin, Compt. Rend. **183**, 24 (1926).

[46] J. B. Keller, Ann. Phys. (N. Y.) **4**, 180 (1958).

[47] A. Einstein, Verh. Dtsch. Phys. Ges. **19**, 82 (1917).

[48] M. C. Gutzwiller, J. Math. Phys. **12**, 343 (1971); and earlier references quoted therein.

[49] R. Balian, and C. Bloch, Ann. Phys. (N. Y.) **69**, 76 (1972).

[50] M. V. Berry and M. Tabor, Proc. R. Soc. Lond. **A 349**, 101 (1976).

[51] M. V. Berry and M. Tabor, Proc. R. Soc. Lond. **A 356**, 375 (1977).

[52] M. C. Gutzwiller: *Chaos in classical and quantum mechanics* (Springer, New York, 1990).

[53] M. Sieber and F. Steiner, Phys. Rev. Lett. **67**, 1941 (1991); M. Sieber, Chaos **2**, 35 (1992).

[54] M. C. Gutzwiller, in *Chaos and quantum physics*, Les Houches Session LII (1989), eds. M.-J. Giannoni *et al.* (North-Holland, Amsterdam, 1991), p. 201.

[55] V. M. Strutinsky, Nukleonika (Poland) **20**, 679 (1975); V. M. Strutinsky and A. G. Magner, Sov. J. Part. Nucl. **7**, 138 (1976); V. M. Strutinsky, A. G. Magner, S. R. Ofengenden, and T. Døssing, Z. Phys. **A 283**, 269 (1977).

[56] S. C. Creagh and R. G. Littlejohn, Phys. Rev. A **44**, 836 (1991); J. Phys. A **25**, 1643 (1992).

[57] J. H. Van Vleck, Proc. Natl. Acad. Sci. USA **14**, 178 (1928).

[58] S. C. Creagh, J. M. Robbins, and R. G. Littlejohn, Phys. Rev. **A 42**, 1907 (1990).

[59] B. Eckhardt and D. Wintgen, J. Phys. A **24**, 4335 (1991).

[60] S. C. Creagh, Ann. Phys. (N. Y.) **248**, 60 (1996).

[61] M. V. Berry and K. E. Mount, Rep. Prog. Phys. **35**, 315 (1972).

[62] V. A. Yakubovich and V. M. Starzhinskii: *Linear differential equations with periodic coefficients*, Vols. 1 and 2 (J. Wiley & Sons, New York, 1975).

[63] M. J. Feigenbaum, J. Stat. Phys. **19**, 25 (1978); Physica **7 D**, 16 (1983).

[64] T. C. Bountis, Physica **3 D**, 577 (1981); J. M. Greene, R. S. McKay, F. Vivaldi, and M. J. Feigenbaum, Physica **3 D**, 468 (1981).

[65] M. Brack, Foundations of Physics **31**, 209 (2001); LANL preprint nlin.CD/0006034.

[66] A. M. Ozorio de Almeida and J. H. Hannay, J. Phys. **A 20**, 5873 (1987); see also A. M. Ozorio de Almeida: *Hamiltonian Systems: Chaos and Quantization* (Cambridge University Press, Cambridge, 1988).

[67] M. Sieber, J. Phys. **A 29**, 4715 (1996); H. Schomerus and M. Sieber, J. Phys. **A 30**, 4537 (1997); M. Sieber and H. Schomerus, J. Phys. **A 31**, 165 (1998); M. Sieber, J. Phys. **A 30**, 4563 (1997).

[68] H. Schomerus, Europhys. Lett. **38**, 423 (1997); J. Phys. **A 31**, 4167 (1998).

[69] S. Tomsovic, M. Grinberg and D. Ullmo, Phys. Rev. Lett **75**, 4346 (1995); see also D. Ullmo, M. Grinberg and S. Tomsovic, Phys. Rev. **E 54**, 135 (1996).

[70] M. Brack, P. Meier, and K. Tanaka, J. Phys. **A 32**, 331 (1999).

[71] A. Magner, S. N. Fedotkin, K. Arita, T. Misu, K. Matsuyanagi, T. Schachner, and M. Brack, Prog. Theor. Phys. (Japan) **102**, 551 (1999).

[72] M. Brack, S. C. Creagh, P. Meier, S. M. Reimann, and M. Seidl, in: *Large Clusters of Atoms and Molecules*, ed. T. P. Martin (Kluwer, Dordrecht, 1996), p. 1.

[73] H. Nishioka, K. Hansen and B. R. Mottelson, Phys. Rev. **B 42**, 9377 (1990).

[74] J. Pedersen, S. Bjørnholm, J. Borggreen, K. Hansen, T. P. Martin, and H. D. Rasmussen, Nature **353**, 733 (1991).

[75] M. Brack, O. Genzken and K. Hansen, Z. Phys. **D 21**, 65 (1991).

[76] M. Pellarin, B. Baguenard, C. Bordas, M. Broyer, J. Lermé, and J. L. Vialle, Phys. Rev. **B 48**, 17645 (1993).

[77] E. Koch and O. Gunnarsson, Phys. Rev. **B 54**, 5168 (1996).

[78] K. Tanaka, S. C. Creagh and M. Brack, Phys. Rev. B **53**, 16050 (1996).

[79] W. D. Knight, K. Clemenger, W. A. de Heer, W. A. Saunders, M. Y. Chou, and M. L. Cohen, Phys. Rev. Lett. **52**, 2141 (1984).

[80] W. D. Knight, K. Clemenger, W. A. de Heer, and W. A. Saunders, Phys. Rev. **B 31**, 2539 (1985).

[81] S. M. Reimann, M. Brack, and K. Hansen, Z. Phys. **D 28**, 235 (1993).

[82] S. M. Reimann and M. Brack, Comp. Mat. Sci. **2**, 433 (1994).

[83] M. Brack and S. R. Jain, Phys. Rev. **A 51**, 3462 (1995).

[84] A. G. Magner, S. N. Fedotkin, F. A. Ivanyuk, P. Meier, M. Brack, S. M. Reimann, and H. Koizumi, Ann. Physik (Leipzig) **6**, 555 (1997); A. G. Magner, S. N. Fedotkin, F. A. Ivanyuk, P. Meier, and M. Brack, Czech. J. Phys. **48**, 845 (1998).

[85] T. Hirschmann, M. Brack, and J. Meyer, Ann. Phys. (Leipzig) **3**, 336 (1994).

[86] P. Meier, M. Brack and S. C. Creagh, Z. Phys. **D 41**, 281 (1997).

[87] K. Richter, Europhys. Lett. **29**, 7 (1995).

[88] G. Hackenbroich and F. von Oppen, Europhys. Lett. **29**, 151 (1995).

[89] M. Persson, J. Pettersson, B. von Sydow, P. E. Lindelof, A. Kristensen, and K. Berggreen, Phys. Rev. **B 52**, 8921 (1995); and earlier references quoted therein.

[90] P. E. Lindelof, P. Hullmann, P. Bøggild, M. Persson, and S. M. Reimann, in: *Large Clusters of Atoms and Molecules*, ed. T. P. Martin (Kluwer, Dordrecht, 1996), p. 89.

[91] S. M. Reimann, M. Persson, P. E. Lindelof, and M. Brack, Z. Phys. **B 101**, 377 (1996).

[92] P. Bøggild, A. Kristensen, P. E. Lindelof, S. M. Reimann, and C. B. Sørensen, in: *8th International Conference on Physics of Semiconductors (ICPS)*, Proceedings (Berlin, 1997), p. 1533.

[93] H. Linke, L. Christensson, P. Omling, and P. E. Lindelof, Phys. Rev. **B 56**, 1440 (1997).

[94] M. Brack, J. Blaschke, S. C. Creagh, A. G. Magner, P. Meier, and S. M. Reimann, Z. Phys. **D 40**, 276 (1997).

[95] M. Hénon and C. Heiles, Astr. J. **69**, 73 (1964).

[96] J. Blaschke and M. Brack, Phys. Rev. **A 56**, 182 (1997); Physica **E1**, 288 (1997).

[97] K. Richter, D. Ullmo and R. A. Jalabert, Phys. Rep. **276**, 1 (1996).

[98] K. Tanaka, Ann. Phys. (N. Y.) **268**, 31 (1998).

[99] J. Blaschke, Ph. D. Thesis (Regensburg University, 1999), available at ⟨http://www.joachim-blaschke.de⟩.

[100] D. Weiss, M. L. Roukes, A. Menschig, P. Grambow, K. von Klitzing, and G. Weimann, Phys. Rev. Lett. **66**, 2790 (1991); D. Weiss, K. Richter, A. Menschig, R. Bergmann, H. Schweizer, K. von Klitzing, and G. Weimann, Phys. Rev. Lett. **70**, 4118 (1993).

[101] D. Weiss and K. Richter, Physica **D 83**, 290 (1995).

[102] C. Gould *et al.*, Phys. Rev. **B 51**, 11213 (1995).

[103] G. Kirczenov *et al.*, Phys. Rev. **56 B**, 7503 (1997).

[104] J. Blaschke and M. Brack, Europhys. Lett. **50**, 294 (2000).

[105] O. Bohigas, A. M. Lane, and J. Martorell, Phys. Rep. **51**, 267 (1979).

[106] P. Gleissl, M. Brack, J. Meyer, and P. Quentin, Ann. Phys. (N. Y.) **197**, 205 (1990).

[107] P.-G. Reinhard, M. Brack, and O. Genzken, Phys. Rev. **A 41**, 5568 (1990).

[108] P.-G. Reinhard and Y. Gambhir, Ann. Phys. (Leipzig) **1**, 598 (1992).

[109] P.-G. Reinhard, O. Genzken, and M. Brack, Ann. Phys. (Leipzig) **5**, 576 (1996).

[110] S. Kümmel, Ph. D. Thesis, Regensburg University: *Structural and Optical Properties of Sodium Clusters Studied in Density Functional Theory* (Logos, Berlin, 2000).

[111] S. Kümmel and M. Brack, Phys. Rev. A **64**, 022506 (2001).

[112] A. L. Fetter and J. D. Walecka: *Quantum theory of many particle systems* (McGraw-Hill, New York, 1971).

[113] A. M. Lane: *Nuclear Theory* (Benjamin, New York, 1964).

[114] D. J. Rowe: *Nuclear collective motion* (Methuen, London, 1970).

[115] G. Vignale und W. Kohn, Phys. Rev. Lett. **77**, 2037 (1996); G. Vignale, C. A. Ullrich, and S. Conti, Phys. Rev. Lett. **79**, 4878 (1997).

[116] J. P. da Providência and G. Holzwarth, Nucl. Phys. **A 398**, 59 (1983); **A 439**, 477 (1985).

[117] G. F. Bertsch, Nucl. Phys. **A 249**, 253 (1975).

[118] H. Sagawa and G. Holzwarth, Prog. Theor. Phys. **59**, 1213 (1978).

[119] D. J. Thouless, Nucl. Phys. **22**, 78 (1961).

[120] E. R. Marshalek and J. P. da Providência, Phys. Rev. **C 7**, 2281 (1973).

[121] T. Hirschmann, M. Brack, and P.-G. Reinhard, Z. Phys. **D 40**, 254 (1997).

[122] S. Kümmel, M. Brack, and P.-G. Reinhard, Phys. Rev. **B 58**, R1774 (1998).

[123] S. Kümmel, M. Brack, and P.-G. Reinhard, Phys. Rev. **B 62**, (Sept. 15) (2000).

[124] C. Yannouleas, M. Brack, R. A. Broglia, and P. F. Bortignon, Phys. Rev. Lett. **63**, 255 (1989).

[125] D. E. Beck, Sol. State Commun. **49**, 381 (1984); Phys. Rev. **B 30**, 6935 (1984).

[126] M. Manninen, R. M. Nieminen, and M. J. Puska, Phys. Rev. **B 33**, 4297 (1986).

[127] S. Kümmel, T. Berkus, P.-G. Reinhard, and M. Brack, Eur. Phys. J. **D 11**, 239 (2000).

[128] D. Rayane *et al.*, Eur. Phys. J. **D 9**, 243 (1999).

[129] S. Kümmel, J. Akola, and M. Manninen, Phys. Rev. Lett. **84**, 3827 (2000).

[130] S. Blundell, C. Guet, and R. R. Zope, Phys. Rev. Lett. **84**, 4826 (2000).

[131] B. Montag and P.-G. Reinhard, Z. Phys. **D 33**, 265 (1995).

[132] S. Kümmel, P.-G. Reinhard, and M. Brack, Eur. Phys. J. **D 9**, 149 (1999).

[133] I. Vasiliev, S. Öğüt, and J. R. Chelikowsky, Phys. Rev. Lett. **82**, 1919 (1999).

[134] W. R. Frederickson and W. W. Watson, Phys. Rev. **30**, 429 (1927); C. R. C. Wang, S. Pollack, D. Cameron, and M. M. Kappes, Chem. Phys. Lett. **166**, 26 (1990).

[135] J. Akola, A. Rytkönen, H. Häkkinen, and M. Manninen, Eur. Phys. J. **D 8**, 93 (2000).

[136] M. Schmidt and H. Haberland, Eur. Phys. J. **D 6**, 109 (1999).